

Non-thermal Origin of Asymmetric Dark Matter from Inflaton and Primordial Black Holes

Basabendu Barman,^{1,*} Debasish Borah,^{2,†} Suruj Jyoti Das,^{2,‡} and Rishav Roshan^{3,§}

¹*Centro de Investigaciones, Universidad Antonio Nariño*

Carrera 3 este # 47A-15, Bogotá, Colombia

²*Department of Physics, Indian Institute of Technology Guwahati, Assam 781039, India*

³*Physical Research Laboratory, Ahmedabad-380009, Gujarat, India*

Abstract

We study the possibility of co-genesis of baryon and dark matter (DM) from the out-of-equilibrium CP violating decay of right handed neutrino (RHN) that are dominantly of non-thermal origin. While the RHN and its heavier partners can take part in light neutrino mass generation via Type-I seesaw mechanism, the decay of RHN into dark and visible sectors can create respective asymmetries simultaneously. The non-thermal sources of RHN considered are **(a)** on-shell decay of inflaton, and **(b)** evaporation of ultralight primordial black holes (PBH). After setting up the complete set of Boltzmann equations in both these scenarios, we constrain the resulting parameter space of the particle physics setup, along with inflaton and PBH sectors from the requirement of generating correct (asymmetric) DM abundance and baryon asymmetry, while being in agreement with other relevant cosmological bounds. Scenario **(a)** links the common origin of DM and baryon asymmetry to post-inflationary reheating via RHNs produced in inflaton decay, whereas in scenario **(b)** we find enhancement of baryon and DM abundance, compared to the purely thermal scenarios, in presence of PBH with appropriate mass and initial fraction. Although the minimal setup itself is very predictive with observational consequences, details of the UV completion of the dark sector can offer several complementary probes.

* basabendu88barman@gmail.com

† dborah@iitg.ac.in

‡ suruj@iitg.ac.in

§ rishav@prl.res.in

CONTENTS

I. Introduction	2
II. The Minimal Setup	5
III. Asymmetric Dark Matter from Inflaton Decay	6
A. Evolution of Yields	9
B. Results and Discussions	12
IV. Asymmetric Dark Matter from PBH evaporation	21
A. Primordial Black Hole: formation and constraints	22
B. Right handed neutrino from PBH: Dark Matter and Baryogenesis	25
C. Results and Discussions	31
V. Possible UV completion of the Dark Sector	37
VI. Conclusion	39
Acknowledgements	40
A. Light neutrino mass & Casas-Ibarra Parametrisation	41
References	42

I. INTRODUCTION

Observational evidences [1–4] suggest that the present universe is composed of about 32% matter out of which only $\sim 5\%$ is in the form of visible matter or baryons. The remaining $\sim 27\%$ is in the form of a mysterious, non-luminous and non-baryonic form of matter, popularly known as the dark matter (DM). In terms of density parameter Ω_{DM} and reduced Hubble constant $h = \text{Hubble Parameter}/(100 \text{ km s}^{-1}\text{Mpc}^{-1})$, the present DM abundance is conventionally reported as [5]

$$\Omega_{\text{DM}}h^2 = 0.120 \pm 0.001 \tag{1}$$

at 68% CL. The visible or baryonic matter content is also highly asymmetric, giving rise to the longstanding puzzle of baryon asymmetry of the universe (BAU). While any non-zero primordial asymmetry chosen as an initial condition will be diluted by the exponentially expanding phase of inflation, it is also natural for the universe to start in a baryon symmetric manner. The observed BAU is quantitatively quoted as the ratio of excess of baryons over anti-baryons to photon [5]

$$\eta_B = \frac{n_B - n_{\bar{B}}}{n_\gamma} \simeq 6.2 \times 10^{-10}. \quad (2)$$

The quoted value of baryon to photon ratio based on the cosmic microwave background (CMB) measurements, agrees with the big bang nucleosynthesis (BBN) estimates as well [6]. While the origin of this asymmetry is not known, the particle nature of DM is also a mystery. However, we do know that none of the standard model (SM) particles satisfy the criteria of a viable particle DM candidate. In addition, the SM also fails to satisfy the criteria (known as Sakharov's conditions [7]) in adequate amounts to dynamically generate the observed BAU. This has led to several beyond the SM (BSM) proposals offering possible solutions to these puzzles. As it is well known, the weakly interacting massive particle (WIMP) paradigm has been the most widely studied particle DM scenario [8–13], while out-of-equilibrium decay of a heavy particle leading to the generation of baryon asymmetry has been a very well known mechanism for baryogenesis [14, 15]. One interesting possibility to achieve baryogenesis via lepton sector physics is known as leptogenesis [16] where, instead of creating a baryon asymmetry directly, a lepton asymmetry is generated first which subsequently gets converted into baryon asymmetry by the $(B + L)$ -violating electroweak sphaleron transitions [17].

The popular BSM frameworks mentioned above can certainly explain the origin of DM and BAU independently, but an intriguing observation is the similarity in their abundances $\Omega_{\text{DM}} \approx 5 \Omega_{\text{Baryon}}$, within the same order of magnitude. Ignoring the possibility of a numerical or mere cosmic coincidence, one has to provide a dynamical origin behind such a serendipity. There have been several works in pursuit of finding a common origin for DM and baryon asymmetry, a brief review of which can be found in [18]. This broadly falls into two categories. In the first one, the usual mechanism for baryogenesis is extended to the dark sector assuming the dark sector to be asymmetric [19–22]. In typical asymmetric dark matter (ADM) scenario, the same out-of-equilibrium decay of a heavy particle into baryon and dark sector can give rise to asymmetries in the two sectors of similar order of magnitudes $n_B - n_{\bar{B}} \sim |n_{\text{DM}} - n_{\bar{\text{DM}}}|$. The second approach is to produce such asymmetries through

annihilations [23–25], where one or more particles involved in the process eventually go out of thermal equilibrium to generate a net asymmetry. The so-called WIMPy baryogenesis [26–28] belongs to this category, where a DM particle freezes out to generate its own relic abundance while simultaneously producing an asymmetry in the baryon sector. The idea extended to leptogenesis is called WIMPy leptogenesis [29–34].

Motivated by these, we consider a simple realisation of the asymmetric dark matter scenario where out-of-equilibrium decay of heavy right handed neutrinos (RHN) can play the role in generating both dark and visible sector asymmetries simultaneously [35, 36]. The same RHNs can also give rise to light neutrino masses via Type-I seesaw mechanism [37–40]. In such generic seesaw models, the scale of thermal leptogenesis remains high pushing the scale of RHN to a very high scale $M > 10^9$ GeV, known as the *Davidson-Ibarra bound* [41]. However, the reheat temperature of the universe after inflation (T_{RH}) can be much lower forbidding the thermal production of RHNs. In such a scenario, the RHNs can still be produced non-thermally from the inflaton field, leading to the scenario of non-thermal leptogenesis [42–60]. Also, there exists no experimental evidence to suggest that the universe was radiation dominated prior to the BBN era and existence of some non-standard cosmological phase can alter the predictions of high scale phenomena like leptogenesis. A recent review of such non-standard cosmology can be found in [61], while its effects on leptogenesis have been discussed in several works including [62–68]. In the present work we consider two different sources of non-thermal RHNs namely, (a) inflaton decay, where we assume that the inflaton decays *only* into a pair of RHNs and (b) evaporation of primordial black holes (PBH), and in each case we study the consequences for generation of dark and visible sector asymmetries. While the first case connects the co-generation of DM and baryons to the post-inflationary reheating via non-thermal RHNs produced from inflaton, the presence of PBH with appropriate mass and initial fraction can lead to enhancement of baryon and asymmetric DM abundance compared to the purely thermal case.

This paper is organised as follows. In section II we discuss our minimal setup. Section III and IV are dedicated to the details of asymmetric dark matter production from inflaton and primordial black holes respectively. In section V, we sketch a possible UV completion of the dark sector, and finally conclude in section VI.

II. THE MINIMAL SETUP

We start with a toy model to motivate our scenario and later provide its possible UV-complete manifestation. The minimum ingredients to generate the dark and visible sector asymmetries are adopted from [35]. The SM particle content is extended by two RHNs sufficient to fit light neutrino data via Type-I seesaw mechanism along with two dark sector particles namely a singlet scalar \mathcal{S} , a singlet Dirac fermion χ both odd under an in-built \mathbb{Z}_2 symmetry. The out-of-equilibrium CP-violating decay of these RHNs to the visible as well as to the dark sector produce asymmetry in both the sectors simultaneously. The interaction Lagrangian for such a scenario can be expressed as

$$-\mathcal{L} \supset \frac{1}{2} M_N \overline{N^c} N + y_N \overline{N} \tilde{H}^\dagger \ell + m_\chi \overline{\chi} \chi + y_\chi \overline{N} \mathcal{S} \chi + \text{h.c.}, \quad (3)$$

where we extend the SM particle spectrum by adding two generations of RHN N_i , singlet under the SM gauge symmetry. The SM leptons are denoted by ℓ . A lepton number is assigned to the RHN such that its Majorana mass term is lepton number violating. Although three copies of RHNs are considered in typical Type-I seesaw model, two are sufficient to fit light neutrino data. The details of light neutrino mass generation and parametrisation of the lepton-RHN coupling in terms of observed parameters of neutrino mass and mixing, are given in Appendix A.

The singlet fermion χ plays the role of viable DM candidate and carries a lepton number same as that of N . We consider this fermion to be vector like such that a bare mass term m_χ can be assigned to it without violating any $U(1)$ symmetry like global lepton number. To ensure the stability of the DM we impose an ad-hoc \mathbb{Z}_2 symmetry under which both the singlet scalar \mathcal{S} and the single fermion χ are odd, while all other particles are even. This also implies, $m_\chi < m_\mathcal{S} < M_i$ such that the singlet fermion is the only DM in the present particle spectrum¹. Note that, the scalar \mathcal{S} is devoid of any vacuum expectation value (VEV) such that there is no mixing between the DM and the RHN that may lead to DM decay². The detailed phenomenology of this minimal setup has been discussed in [35] by considering thermal RHNs. For thermal RHNs, the subsequent phenomenology is

¹Possibility of either of them to be DM, depending on the mass hierarchy, has been addressed in [35].

²Non-zero VEV can result in DM decay into SM states that can have observational consequences [35, 69].

insensitive to early universe histories. In this work, we consider non-thermal RHNs to be the dominant source of asymmetries. As we discuss below, inflaton and primordial black holes can play non-trivial roles in producing such non-thermal RHNs in the early universe leading to subsequent asymmetries in visible and dark sectors.

III. ASYMMETRIC DARK MATTER FROM INFLATON DECAY

In the standard vanilla leptogenesis [70] as well as in minimal ADM framework, the decaying particles (RHNs in our setup) are produced thermally from the SM bath. However, the lower bound on RHN mass in such scenarios (Davidson-Ibarra bound, mentioned before), leads to a lower bound on the reheat temperature $T_{\text{RH}} \geq 10^{10}$ GeV [41, 71] so that the RHNs can be produced from the thermal bath. While there is no observational evidence to suggest such a high reheat temperature, one also faces the gravitino overproduction problem in supersymmetric scenarios for such high T_{RH} [72]. One suitable alternative is to consider non-thermal production of RHNs. In this section, we consider the inflaton decay into RHNs as a possible source. Our set-up is based on the assumption that the inflaton field φ decays *only* into a pair of RHNs [42, 60, 73] via the coupling

$$- \mathcal{L} \supset y_\varphi \varphi \overline{N^c} N, \quad (4)$$

We consider inflaton coupling to other particles like DM χ : $\varphi \overline{\chi} \chi$, singlet scalar \mathcal{S} : $\varphi \mathcal{S} \mathcal{S}$, SM Higgs H : $\varphi H^\dagger H$ to be absent for simplicity. This ensures the inflaton to transfer its entire energy density into the RHNs which subsequently decays into other light degrees of freedom (DOF), leading to the required reheating of the universe. Without going into the details of the dynamics of inflation, in the present scenario we look into the post slow-roll era when the inflaton energy starts converting into the energy of the heavy neutrinos. This helps us to perform the analysis without worrying about the details of inflationary model or inflation potential. Similar approach can be found in [74] which considered the separation of the period of inflation from reheating along with references for specific models of inflation which allow this possibility.

As advocated in the beginning, we are interested in the scenario where the asymmetry in the visible and in the DM sector are simultaneously generated from the non-thermal decay of

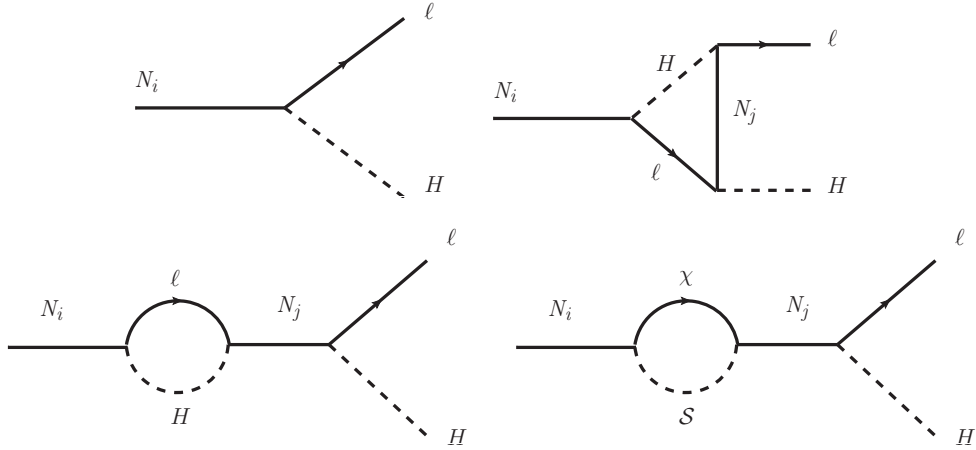


Figure 1. Tree level, vertex and the self-energy diagrams required for the generation of the asymmetry in the lepton sector.

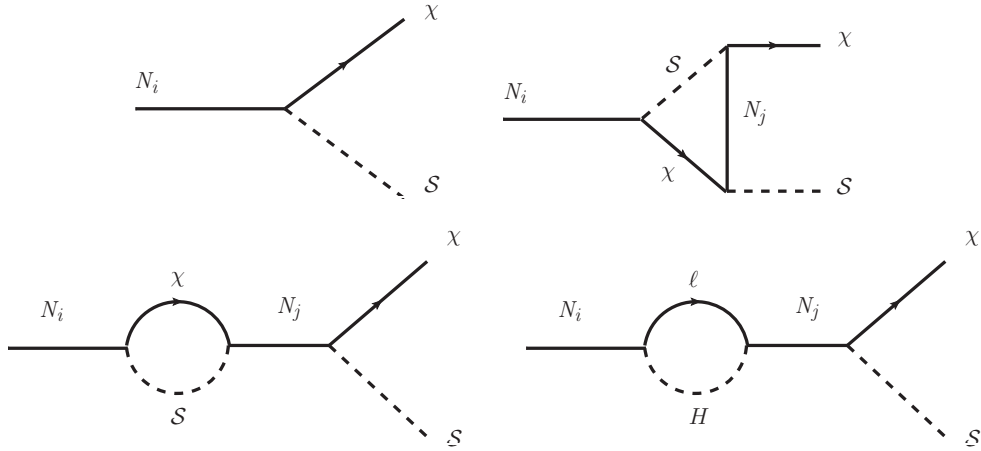


Figure 2. Same as Fig. 1 but for the generation of the asymmetry in the dark sector.

RHNs where the latter originate solely from the decay of inflaton. Assuming the symmetric component of the DM being washed out, it is the asymmetry $n_\chi - n_{\bar{\chi}}$ in number densities of DM particles that determines the DM abundance in late universe. Since the DM χ carries a lepton number, hence lepton number asymmetries are generated in both the sector. We also assume $M_1 \ll M_2$ i.e, we can integrate out N_2 and consider contribution only from N_1 decay. The decay of N_1 to the SM final states also generate the thermal bath in this process. In Fig. 1 and Fig. 2 we depict the relevant Feynman diagrams that generate these asymmetries. Below we express the CP asymmetries produced in the two sectors from the

decay of the lightest RHN N_1 [35]:

$$\epsilon_{\Delta L} = \frac{\sum_{\alpha} [\Gamma(N_1 \rightarrow l_{\alpha} + H) - \Gamma(N_1 \rightarrow \bar{l}_{\alpha} + H^*)]}{\Gamma_1} \quad (5)$$

$$\simeq \frac{M_1}{8\pi} \frac{\text{Im}[(3 y_N^* y_N^T + y_{\chi}^* y_{\chi}^T) M^{-1}, y_N y_N^{\dagger}]_{11}}{[2 y_N y_N^{\dagger} + y_{\chi} y_{\chi}^{\dagger}]_{11}}, \quad (6)$$

and

$$\epsilon_{\Delta \chi} = \frac{\Gamma(N_1 \rightarrow \chi + S) - \Gamma(N_1 \rightarrow \bar{\chi} + S^*)}{\Gamma_1} \quad (7)$$

$$\simeq \frac{M_1}{8\pi} \frac{\text{Im}[(y_N^* y_N^T + y_{\chi}^* y_{\chi}^T) M^{-1} y_{\chi} y_{\chi}^{\dagger}]_{11}}{[2 y_N y_N^{\dagger} + y_{\chi} y_{\chi}^{\dagger}]_{11}}, \quad (8)$$

where

$$\Gamma_1 = \frac{M_1}{16\pi} (2 y_N y_N^{\dagger} + y_{\chi} y_{\chi}^{\dagger})_{11}, \quad (9)$$

is the total decay width of N_1 and $M = \text{diag}(M_1, M_2)$ is the diagonal RHN mass matrix considering two RHNs. We choose hierarchical RHN mass spectrum with $M_2 = 50 M_1$ such that the inflaton only decays into N_1 . Since we have a single generation of χ , the y_{χ} matrix can be taken, in general, to be of the form

$$y_{\chi} = \begin{pmatrix} y_{\chi 1} \\ y_{\chi 2} \end{pmatrix}. \quad (10)$$

For the analysis purpose, we assume $y_{\chi i}$ to be real and identical, denoted by y_{χ} . It is noteworthy that even with real y_{χ} we are being able to generate adequate CP-violation thanks to the complex Yukawa couplings in the visible sector. Moreover, relative difference in the two asymmetries depend upon the branching ratio of N_1 decay and the washout, transfer effects in case of thermal leptogenesis. However, since we are considering non-thermal leptogenesis scenario where the RHN mass is larger than the reheating temperature, these effects are sub-dominant and we ignore them in our analysis.

A. Evolution of Yields

Since inflaton decays into RHNs only which subsequently decays into radiation while producing dark and visible sector asymmetries at the same time, it is expected that the evolution of yields for different components are interlinked, and can be expressed in terms of a set of coupled Boltzmann equations (BEQ). This is given in Eq. (11). The setup can also be understood from the cartoon in Fig. 3, where we show how different components are linked to each other. The set of coupled BEQs governing the evolution of energy densities together with the dark and visible sector asymmetries is given by

$$\begin{aligned}
\dot{\rho}_\varphi &= -3\mathcal{H}\rho_\varphi - \Gamma_\varphi\rho_\varphi \\
\dot{\rho}_N &= -3\mathcal{H}\rho_N + \Gamma_\varphi\rho_\varphi - \Gamma_N\rho_N \\
\dot{n}_{\text{B-L}} &= -3\mathcal{H}n_{\text{B-L}} - \epsilon_{\Delta\text{L}}\Gamma_N n_N - \Gamma_{\text{ID}}n_{\text{B-L}} \\
\dot{\rho}_R &= -4\mathcal{H}\rho_R + \Gamma_N\rho_N \\
\dot{n}_{\Delta\chi} &= -3\mathcal{H}n_{\Delta\chi} + \epsilon_{\Delta\chi}\Gamma_N n_N - \Gamma_{\text{ID}}n_{\Delta\chi}
\end{aligned} \tag{11}$$

where Γ_{ID} is the inverse decay rate. As $M_1 \gtrsim T_{\text{RH}}$, here onward we are going to ignore Γ_{ID} as the bath does not have enough energy to produce the RHNs from SM reaction. By the same argument, scattering processes causing washouts of the produced asymmetries can also be ignored. The third and the fifth equations determine the yield for the visible and dark sector asymmetries respectively, while the first, second and fourth equations determine the evolution of the energy densities for the inflaton, RHN and radiation respectively. As the RHNs are non-relativistic, therefore $n_N = \rho_N/m_N$ holds, where in our case $m_N \equiv M_1$. The inflaton decays *only* into a pair of lightest RHNs, the decay width is thus given by

$$\Gamma_\varphi \simeq \frac{y_\varphi^2}{4\pi} m_\varphi. \tag{12}$$

Since we are considering a hierarchical mass spectrum for the heavy neutrinos $M_2 \gg M_1$ (with $2M_1 < m_\varphi$), hence potential effects of N_2 can be neglected³.

³Baryon asymmetry can be generated by the second-lightest RHN in certain areas of parameter space as discussed in the context of thermal leptogenesis [75].

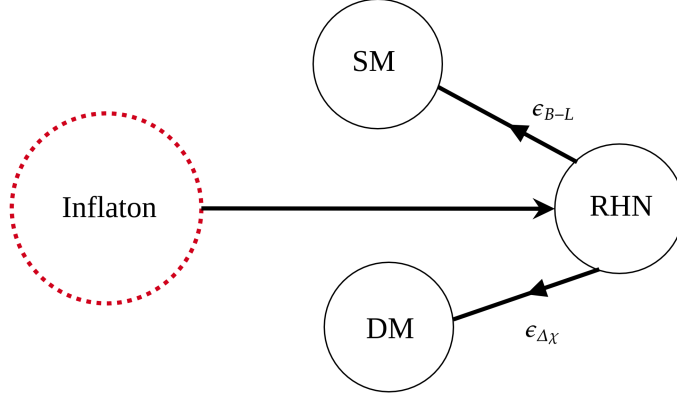


Figure 3. Schematic diagram of asymmetry production in the dark and in the visible sector from RHN produced from inflaton decay.

It is convenient to make suitable variable transformation while solving Eq. (11). We make the following set of transformations by scaling the energy and number densities with the scale factor a [55, 76]

$$\begin{aligned}
 \tilde{\rho}_\varphi &= \rho_\varphi a^3, \\
 \tilde{\rho}_N &= \rho_N a^3, \\
 \tilde{N}_{B-L} &= n_{B-L} a^3, \\
 \tilde{\rho}_R &= \rho_R a^4, \\
 X &= n_{\Delta\chi} a^3.
 \end{aligned} \tag{13}$$

We also define

$$\xi = \frac{a}{a_I}$$

as the ratio of scale factors and assume $a_I = 1$. Note that, no physical result depends on this choice and hence a_I can be chosen to be anything⁴. The factor a_I is chosen as the initial value of the scale factor, while ξ is the proxy to the time (temperature) variable. With these definitions, the Hubble parameter reads

$$\mathcal{H} = \sqrt{\frac{8\pi}{3M_{\text{pl}}^2} \frac{\tilde{\rho}_\varphi a_I \xi + \tilde{\rho}_N a_I \xi + \tilde{\rho}_R}{a_I^4 \xi^4}}. \tag{14}$$

⁴In [76], the authors have defined $a_I = T_{\text{RH}}^{-1}$.

In terms of these rescaled variables, Eq. (11) can be written as

$$\begin{aligned}
\tilde{\rho}_\varphi &= -\frac{\Gamma_\varphi}{\mathcal{H}} \frac{\tilde{\rho}_\varphi}{\xi}, \\
\tilde{\rho}_N &= \frac{\Gamma_\varphi}{\mathcal{H}} \frac{\tilde{\rho}_\varphi}{\xi} - \frac{\Gamma_N}{\mathcal{H}\xi} \tilde{\rho}_N, \\
\tilde{N}'_{B-L} &= \frac{\Gamma_N}{\mathcal{H}\xi} \epsilon_{\Delta L} \frac{\tilde{\rho}_N}{M_1}, \\
\tilde{\rho}_R &= \frac{\Gamma_N a_I}{\mathcal{H}} \tilde{\rho}_N, \\
X' &= \frac{\Gamma_N}{\mathcal{H}\xi} \epsilon_{\Delta X} \frac{\tilde{\rho}_N}{M_1}.
\end{aligned} \tag{15}$$

In the above set of equations, prime in superscript corresponds to derivative with respect to $\xi = a/a_I$. Excepting for the inflaton, which has an initial energy density, all other quantities are being produced from different sources originating directly or indirectly from inflaton only. Hence we can set the initial conditions for different quantities appearing in Eq. (15) as

$$\begin{aligned}
\tilde{N}_{(B-L)I} &= 0; \quad \tilde{\rho}_\varphi = \tilde{\rho}_{\varphi I}; \\
\tilde{\rho}_{R_I} &= 0; \quad \tilde{\rho}_{N_I} = 0; \quad X_I = 0.
\end{aligned} \tag{16}$$

In obtaining the initial energy density for the inflaton we use

$$\tilde{\rho}_{\varphi I} = \frac{3}{8\pi} M_{\text{pl}}^2 H_I^2 \equiv \rho_{\varphi I}, \tag{17}$$

where the last line follows from the fact that $a_I = 1$. Now, CMB observation puts a bound on the scale of inflation [77]: $H_I < 2.5 \times 10^{-5} M_{\text{pl}}$, implying $\rho_{\varphi I} \lesssim 3 \times 10^{-6} M_{\text{pl}}^4$. The observed baryon asymmetry depends on the final $B - L$ abundance, which can be derived in terms of the redefined \tilde{N}_{B-L} via

$$Y_{B-L} = \frac{n_{B-L}}{s} = \left[\frac{45}{2\pi^2 g_{\star s}} \right] \left(\frac{30}{\pi^2 g_{\star \rho}} \right)^{-3/4} \tilde{N}_{B-L} \tilde{\rho}_R^{-3/4}, \tag{18}$$

where we have used

$$T = \left(\frac{30\rho_R}{\pi^2 g_\star} \right)^{1/4} \tag{19}$$

which is allowed since the heavy neutrinos are non-relativistic⁵. Sphaleron interactions are in equilibrium in the temperature range between ~ 100 GeV and 10^{12} GeV, and they convert a fraction of a non-zero $B - L$ asymmetry into a baryon asymmetry via

$$Y_B \simeq a_{\text{sph}} Y_{B-L} = \frac{8 N_F + 4 N_H}{22 N_F + 13 N_H} Y_{B-L}, \quad (20)$$

where N_F is the number of fermion generations and N_H is the number of Higgs doublets, which in our case $N_F = 3$, $N_H = 1$ and a_{sph} turns out to be $28/79$. In leptogenesis, where purely a lepton asymmetry is generated, $B - L = -L$. This is converted into the baryon asymmetry via sphaleron transition [70, 71]. Finally, the observed baryon asymmetry of the universe is given by [77]

$$\eta_B = \frac{n_B - n_{\bar{B}}}{n_\gamma} \simeq 6.2 \times 10^{-10}, Y_B \simeq 8.7 \times 10^{-11}. \quad (21)$$

As mentioned before, the DM abundance is set by the asymmetry in the DM sector that indicates the residual number density for the asymmetric DM, and is given by

$$\Omega_\chi h^2 \simeq 2.75 \times 10^8 \left(\frac{m_\chi}{\text{GeV}} \right) \mathcal{Y}_{\Delta\chi}(T_0) = 2.75 \times 10^8 m_\chi X \tilde{\rho}_R^{-3/4} \left(\frac{45}{2 \pi^2 g_{*s}} \right) \left(\frac{\pi^2 g_{*\rho}}{30} \right)^{3/4} \quad (22)$$

where $\mathcal{Y}_{\Delta\chi}(T_0) \equiv n_{\Delta\chi}/s(T_0)$ is the yield of the asymmetry in the DM sector at the present temperature T_0 and s is the entropy per comoving volume in the visible sector.

B. Results and Discussions

In this section we discuss the results of the first part of our analysis i.e., asymmetric DM from inflaton decay. The solution to the set of five coupled BEQ in Eq. (15) is numerically performed to obtain the yield of the different components. Note that, the minimal model provides us with the following free parameters

$$\{M_1, m_\varphi, m_\chi, y_\chi, y_\varphi\}. \quad (23)$$

⁵If the produced heavy neutrinos were relativistic then $T = \left(\frac{30(\rho_R + \rho_N)}{\pi^2 g_*} \right)^{1/4}$, which would be true if $m_\varphi \gg M_N$.

However, in the following analysis we will always fix the mass of the inflaton and the RHN ensuring $M_1 < m_\varphi/2$ such that the inflaton can always decay into a pair of RHNs on-shell. Hence the resulting parameter space is decided by three free parameters, namely the Yukawas $y_{\chi,\varphi}$ and the DM mass m_χ . Before delving into a detailed parameter space scan, we first analyze the impact of different free parameters on the yield by fixing a few of them to benchmark values.

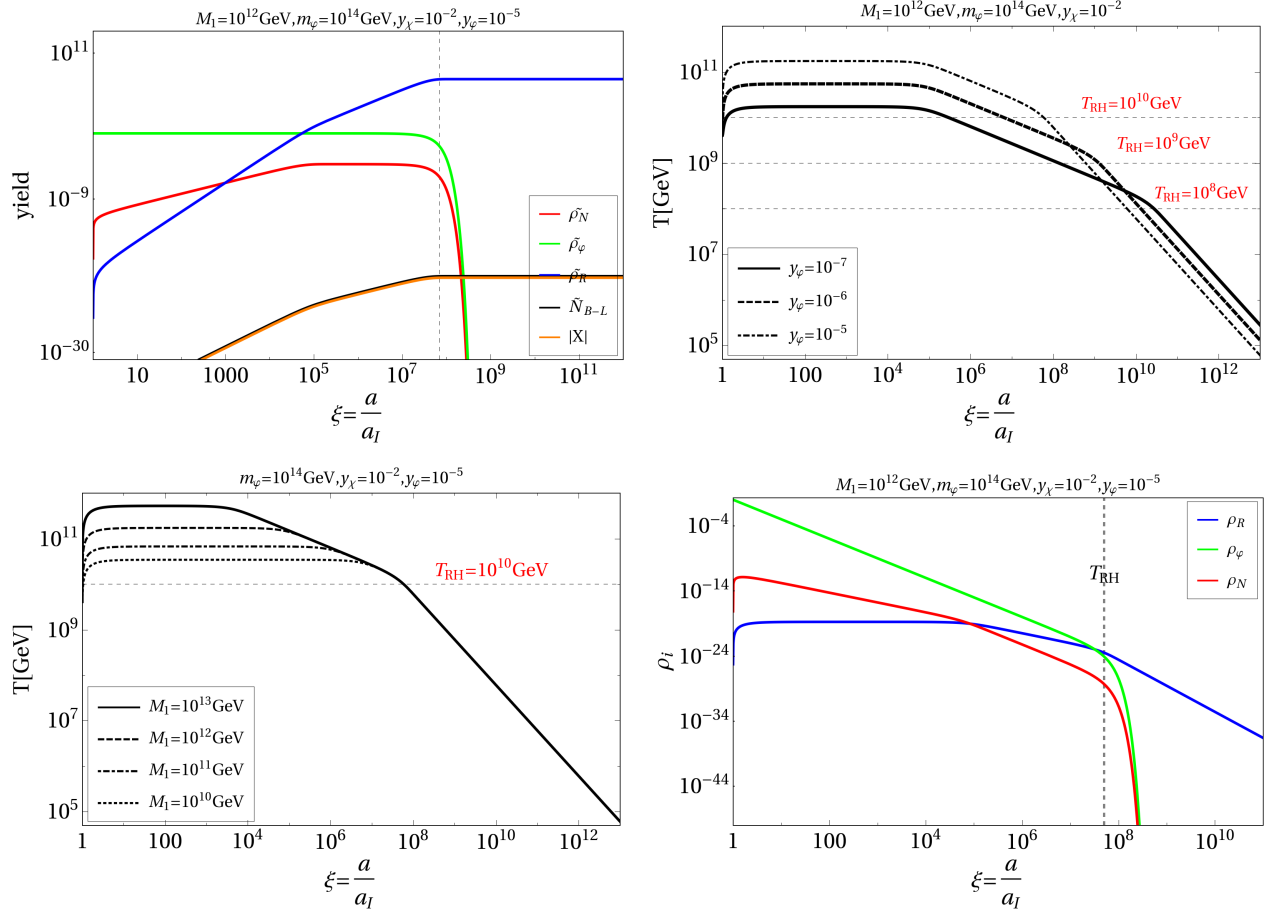


Figure 4. Top left panel: Yield of different components (normalized to $\tilde{\rho}_{\varphi I}$) as a function of $\xi = a/a_I$ for fixed values of the RHN mass $M_1 = 10^{12}$ GeV, inflaton mass $m_\varphi = 10^{14}$ GeV and Yukawas $y_\chi = 10^{-2}, y_\varphi = 10^{-5}$. Top right panel: Evolution of SM bath temperature T with $\xi = a/a_I$ for different choices of y_φ shown by different patterns. Bottom left panel: Same as top right panel but with different choices of the RHN mass shown by different curves. Bottom right panel: Energy densities as function of ξ for fixed choices of other parameters as mentioned in the plot.

In the top left panel of Fig. 4 we show yields as function of $\xi = a/a_I$ for $M_1 = 10^{12}$

GeV, $m_\varphi = 10^{14}$ GeV, $y_\chi = 10^{-2}$ and $y_\varphi = 10^{-5}$. These choices are arbitrary and a different combination can also lead to the observed relic abundance for the DM or the baryon asymmetry of the universe. Here we see, as expected, the yields for radiation (in blue) and the asymmetries (in black and orange) start from very small values initially and then increase with time, whereas the same for the inflaton and the RHN diminish. In fact the RHN abundance also increases from small values at very early epochs, after the inflaton field starts decaying into them. The yields for radiation and asymmetries get saturated at $\xi \sim 6.5 \times 10^7$. This corresponds to the reheating temperature $T_{\text{RH}} \simeq 10^{10}$ GeV as one can read off from the top right panel plot where we show the evolution of SM bath temperature with the scale factor. Needless to mention, at $T = T_{\text{RH}}$ inflaton decay is completed and the universe enters into radiation dominated era. As a result, the radiation yield also saturate at the same time, as shown by the blue curve in top left panel plot. The completion of inflaton decay also implies that the RHNs do not get produced further beyond $\xi \sim 6.5 \times 10^7$, since the inflaton has a 100% decay into the RHNs. Hence we see a sharp fall in the RHN yield (shown via red curve) due to its decay into leptons and DM. Consequently, the asymmetries both in the visible and the DM sector freeze in at the same time (shown in black and orange colour). This is interesting since inflaton decay plays the key role in deciding the dynamics of different components. One must also notice a bend near $\xi \sim 5.2 \times 10^4$ in the yields for the RHN (and the asymmetries). Beyond this point the production of the RHNs via $\varphi \rightarrow N_1 N_1$ process becomes comparable to its decay. As a consequence, we see a plateau region in RHN evolution before its yield starts falling sharply at $T = T_{\text{RH}}$, where the inflaton decay is over. Since RHN is the source for both the radiation and the asymmetries, hence we see a change in slopes of blue, black and orange coloured curves near $\xi \sim 5.2 \times 10^4$. This practically corresponds to the maximum temperature attainable during reheating i.e., $T = T_{\text{max}}$. Finally, note that the asymmetries in either sector evolve exactly in the same manner, since they have the same source. In the top right panel the evolution of the SM temperature is plotted against ξ , where we clearly see the effect of non-instantaneous decay of the inflaton, due to which the bath temperature rises up to $T = T_{\text{max}}$ at a very early time. One should note, for a given y_φ , initially, the temperature is independent of ξ (for $y_\varphi = 10^{-5}$ this happens till $\xi \sim 10^5$). During this time the RHN number density is large enough such that $\Gamma_N \rho_N$ (for a given M_1 , Γ_N is fixed) becomes comparable to $4\mathcal{H}\rho_R$ that accounts for the dilution of radiation energy density due to expansion. Hence we do not

see any visible change in the bath temperature as the radiation energy density remains approximately constant with time during this period cf. second equation in Eq. (11). The temperature then evolves as $T \propto a^{-3/8}$, when the RHN decay rate becomes comparable to its production rate, as a consequence the RHN yield stops increasing further after a certain ξ depending on y_φ (for $y_\varphi = 10^{-5}$ we see this pattern between $\xi \sim 10^5 - 10^7$), but the decay still goes on. Afterward, the temperature scales as $T \propto a^{-1}$ when the inflaton decay to RHN is complete, as a result of which subsequent RHN production ceases and there is no further production of radiation bath. This is where the radiation dominated era begins. The change of slope at $T = T_{\text{RH}}$ denotes this transition. Note that, a smaller y_φ results in a smaller reheating temperature. This is expected since a larger y_φ results in a larger decay width $\Gamma_{\varphi \rightarrow N_1 N_1} \propto y_\varphi^2$ for the inflaton, giving rise to a smaller lifetime. This means the inflaton decay is complete earlier and radiation domination begins at a higher temperature i.e., a higher T_{RH} . On the other hand, for a fixed y_φ , the evolution of SM bath temperature does not get affected for different y_χ since it does not affect the inflaton decay width. The plateau becomes wider with smaller RHN mass since in that case the decay of the RHN is delayed and the RHN-dominated epoch gets longer as shown in the bottom left panel. It is important to note here that for fixed y_φ and y_χ , the ratio of T_{RH} to T_{max} is fixed, and not a free parameter. We find, in our scenario $T_{\text{max}}/T_{\text{RH}}$ can be maximum of $\sim \mathcal{O}(100)$ for $y_\varphi = 10^{-7}$, while for larger y_φ , this ratio can be of $\sim \mathcal{O}(10)$ as can be seen from top right panel of Fig. 4. Note that, with the chosen values of y_φ we always have $\Gamma_\varphi \ll \Gamma_N$, therefore the RHNs decay instantaneously after having been produced in inflaton decays, implying the RHN dominated epoch occurs over a very short period of time. Lastly, in the bottom right panel we show the evolution of energy densities (scaled with respect to the initial inflaton energy density) of radiation, inflaton and RHN with ξ . The importance of this plot lies in the fact that the energy density due to radiation dominates over that due to inflaton at and after $\xi \sim 5.2 \times 10^7$, which, in other words, is the point beyond which the temperature scales as a^{-1} i.e., radiation dominated era begins. This boundary is exactly where we can define the reheating temperature T_{RH} , as can be read off from the top right panel (dot-dashed curve).

The effect of the free parameters on the yield of DM and $B - L$ asymmetry are illustrated in Fig. 5. We again fix the RHN mass $M_1 = 10^{12}$ GeV and the inflaton mass to $m_\varphi = 10^{14}$ GeV. Then we plot the asymmetries as a function of $\xi = a/a_I$ considering different values

of the Yukawas $\{y_\chi, y_\varphi\}$. In the top left panel we show how the DM asymmetry varies with ξ for a fixed y_χ with different choices of y_φ shown in different colours. Here we see, irrespective of the choice of y_φ , the asymptotic DM asymmetry remains the same. This is because, the asymmetry in the DM sector $X' \propto \epsilon_{\Delta\chi} \propto y_\chi^2$ (Eq. (15)), hence for a fixed y_χ the final asymmetry does not change. However, a larger y_φ results in a larger decay width or equivalently, a shorter lifetime for the inflaton. As a consequence, we see the inflaton abundance falls earlier for a larger y_φ (red dot-dashed curve) showing a smaller plateau. This also, in turn, affects the RHN yield. For a smaller y_φ (that correspond to a smaller T_{RH}) we see a wider plateau in $\tilde{\rho}_N$ (blue dashed curve). As in this case, the inflaton decay occurs over a longer period, the RHN production remains comparable to its decay over a longer epoch. For larger y_φ the RHN yield also rises compared to other cases since $\tilde{\rho}_N \propto \Gamma_\varphi \propto y_\varphi^2$. Since the RHN mass is fixed (so is the Dirac Yukawa coupling), hence the final $B - L$ asymmetries also converge for different choices of y_φ as seen from the top right panel plot. Note that, both the yield X and \tilde{N}_{B-L} increase initially with the increase in y_φ , simply because the RHN yield rises. But as soon as the inflaton decay gets completed they converge to fixed asymptotic values. Similar to the behaviour seen in Fig. 4, we again see the asymmetries saturating the moment inflaton decay is complete. In the middle panel we show the dependence of relevant yields on y_χ , by keeping y_φ fixed to a constant value. Here we find, increasing y_χ results in an enhanced DM asymmetry but has a negligible effect on $B - L$ asymmetry. Since y_φ is kept fixed (along with RHN mass), the inflaton decay width also remains fixed due to which there is no visible change in $\tilde{\rho}_\varphi$ (blue dot-dashed curve). The influence of y_χ on $B - L$ asymmetry is even minute as shown by the middle right panel plot, where different coloured solid curves are almost inseparable. Finally in the bottom panel we show the effect of having different RHN masses keeping the Yukawas fixed. First of all, here we see, different masses of the RHNs do not affect the evolution of inflaton energy density since the inflaton decay width remains approximately unchanged. However, a smaller M_1 results in a smaller plateau for the RHN (as shown by the red dashed curve) yield. This can be attributed to the fact that for heavier RHN, the corresponding Dirac Yukawa coupling is comparatively large, hence its decay starts competing with the production from a much earlier epoch leading to a wider plateau region. However, the RHN decay gets completed at the same time immaterial of their masses because of the fact that the reheating temperature remains fixed for a fixed y_φ . Also, for a low mass RHN, the yield

in its density is larger since a smaller mass results in a smaller decay width which in turn implies that the decay rate starts competing with the production at a much later epoch. This results in a larger yield for RHN with smaller mass. Since a larger M_1 corresponds to a larger Dirac Yukawa coupling, hence the branching ratio of N_1 decay to SM final states become dominant when M_1 is comparatively large. This reduces the final DM yield as one can see from the solid curves in the bottom left panel. On the other hand, different M_1 's do not affect the asymptotic yield of the $B - L$ asymmetry as one can see from the bottom right panel plot, since for a fixed y_φ , the reheating temperature T_{RH} does not change, and so is the inflaton decay width. Therefore, the $B - L$ production stops as soon the inflaton decay is complete irrespective of RHN mass. Before moving on we would like to mention that the final baryon asymmetry in the present scenario can be analytically determined, assuming the inflaton decays instantaneously after getting produced from inflaton decay as [42, 45–48]

$$Y_B \simeq -\frac{28}{79} \frac{3}{2} \epsilon_1 \frac{T_{\text{RH}}}{m_\varphi}. \quad (24)$$

We find, using $y_\varphi = 10^{-7}$, $y_\chi = 10^{-2}$, $M_1 = 10^{12}$ GeV and $m_\varphi = 10^{14}$ GeV our full numerical calculation provides $Y_B^{\text{numerical}} = 4.75 \times 10^{-12}$, whereas from the approximately analytical expression we obtain $Y_B^{\text{analytical}} = 4.25 \times 10^{-13}$ for $T_{\text{RH}} \simeq 10^9$ GeV. The difference of $\sim \mathcal{O}(1)$ in the magnitude of final baryon asymmetry is expected since in the full numerical analysis we have considered the effect of $T_{\text{max}}(> T_{\text{RH}})$ incorporating the non-instantaneous inflaton decay.

In Fig. 6 we have shown how the asymmetries in the visible (top panel) and in the DM sector (bottom panel) evolve with time. We have fixed the RHN and the inflaton mass to 10^{12} GeV and 10^{14} GeV respectively, while considering some benchmark values of the Yukawa couplings y_χ and y_φ to understand their effects. For a fixed y_φ , radiation and inflaton energy densities are not affected by different choices of y_χ as one can notice from the top left figure. However, the $B - L$ asymmetry slightly rises for increase in y_χ since it altogether increases RHN decay width although the branching in the visible sector gets diminished. One should note the change in slope of all the solid curves at $\xi \sim 10^7$, where the inflaton decay is complete. This change in slope in n_{B-L}/s is due to the decay of the RHN that results in entropy injection in the thermal plasma, which stops at $\xi \sim 10^8$ once the RHN decay is complete and thereafter remains constant till today. On the other hand,

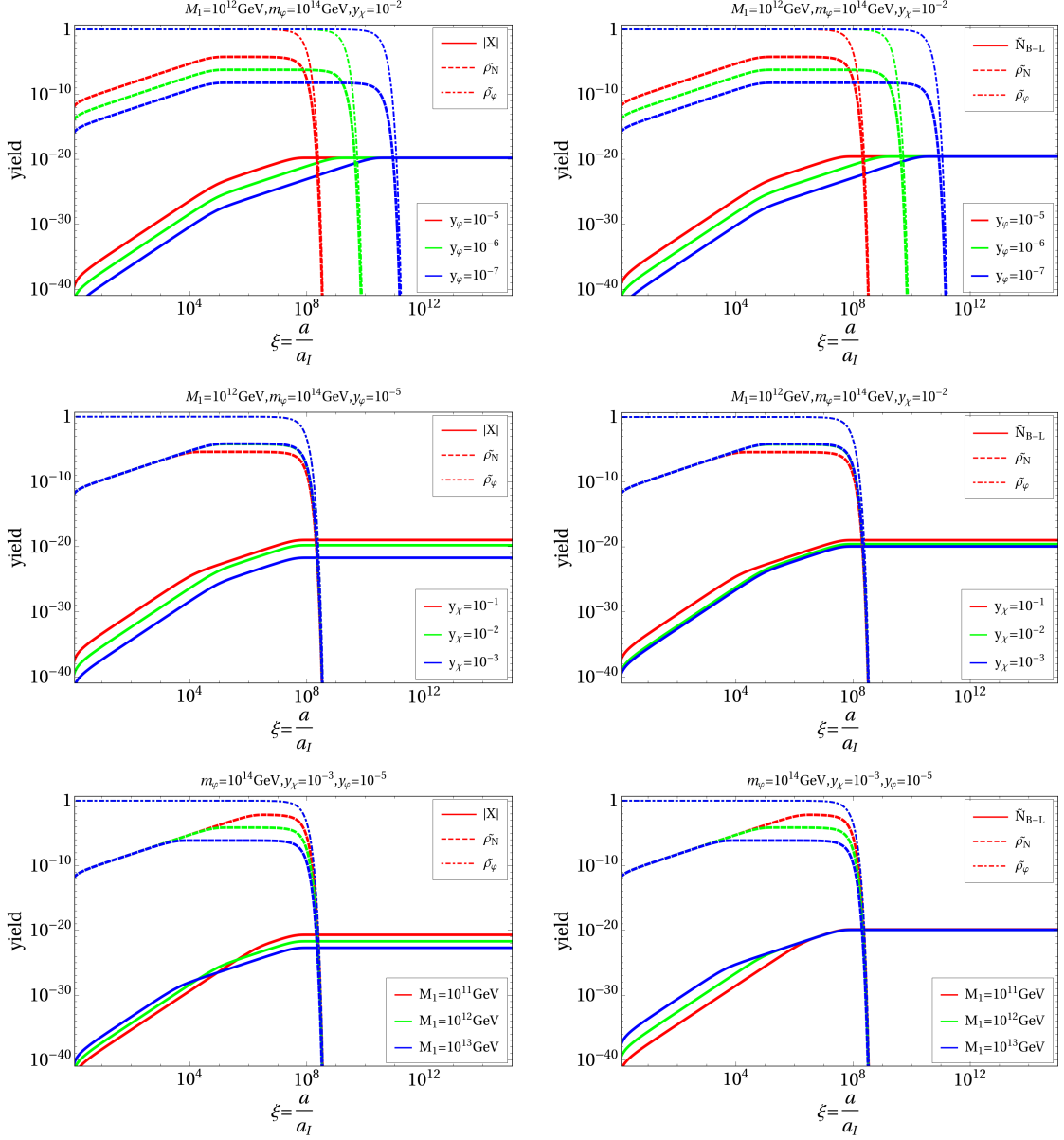


Figure 5. Top panel: Variation of inflaton energy, radiation energy, together with the DM asymmetry (left panel) and $B - L$ asymmetry (right panel) shown respectively by dot-dashed, dashed and solid curves (normalized to $\tilde{\rho}_{\varphi I}$). Here different colours correspond to different choices of y_φ , while y_χ is kept fixed along with the mass of the RHN. Middle panel: Same as top panel but for different choices of y_χ shown in different colours, while y_φ is kept to a fixed value. Bottom panel: Same as top and middle but for different choices of the RHN mass M_1 shown in different colours, where $y_{\chi,\varphi}$ are fixed. In all these plots the inflaton mass is fixed to $m_\varphi = 10^{14}$ GeV.

different choices of y_φ potentially affect the decay lifetime of the inflaton causing it to decay

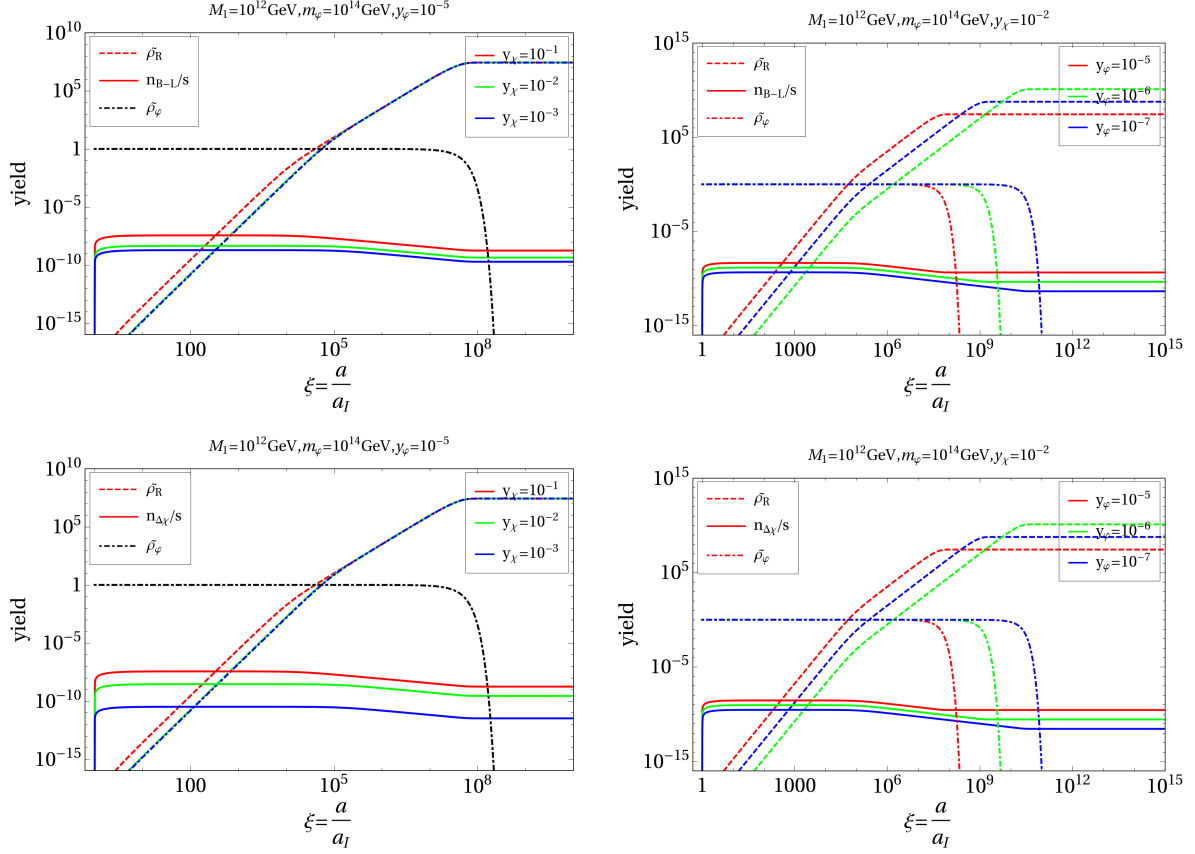


Figure 6. Top panel: Evolution of radiation, inflaton energy density and $B - L$ asymmetry with ξ for different choices of y_χ (left) and y_φ (right) shown in different colours. Bottom panel: Same as top but with asymmetry in the DM sector.

faster for a larger y_φ . This is evident from the red dot-dashed curve in the top right panel. Here the change of slope in the solid curves are even more prominent and they occur at different epoch as the decay lifetime of the inflaton keeps changing with y_φ . Again because of the common single source of asymmetry we find $n_{\Delta\chi}/s$ to behave exactly in the same manner as n_{B-L}/s , as one can perceive from the bottom panel plots. Therefore we do not elaborate them further.

Finally, a scan of the viable parameter space can be done by varying the DM mass and the two Yukawa couplings over the ranges

$$m_\chi : \{1 - 10^8\} \text{ GeV}; y_\chi : \{10^{-4} - 10^{-1}\}; y_\varphi : \{10^{-7} - 10^{-5}\}, \quad (25)$$

to satisfy both right relic abundance for the DM and also to produce the observed baryon

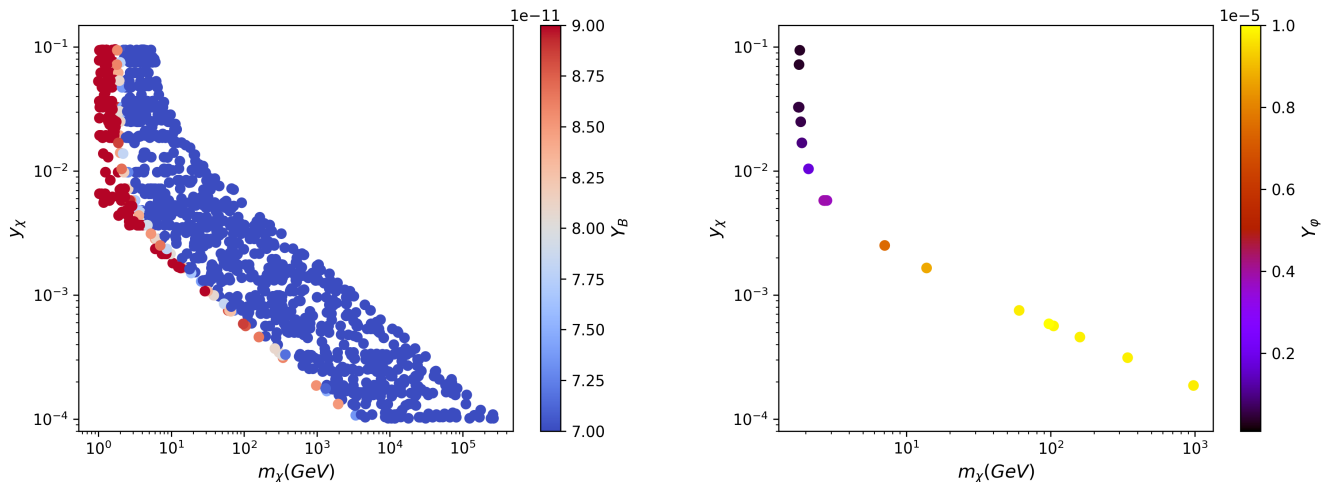


Figure 7. Left panel: Relic density allowed parameter space in $y_\chi - m_\chi$ plane where the colour bar shows the variation of Y_B , while all the points satisfy Planck observed relic abundance in the range $0.119 \leq \Omega_\chi h^2 \leq 0.122$. Right panel: Parameter space satisfying relic density and observed baryon asymmetry for $8.52 \times 10^{-11} \leq Y_B \leq 8.98 \times 10^{-11}$, where the colour code shows values of y_ϕ . Here we have fixed $M_1 = 10^{12}$ GeV and $m_\phi = 10^{14}$ GeV.

asymmetry. The range of y_ϕ is chosen in such a way that $\Gamma_\phi \ll \Gamma_N$, and the universe has a very short RHN dominated epoch. One should also note, within this range of y_ϕ , the reheating temperature of the universe $T_{\text{RH}} \leq 10^{10}$ GeV that satisfies the condition for non-thermal leptogenesis since we are choosing $M_1 = 10^{12}$ GeV for all these scans. All coloured points in the left panel plot of Fig. 7 satisfy the Planck observed relic abundance of DM. Now, increasing y_χ results in a larger asymmetry in the DM sector because of larger branching ratio of corresponding N_1 decay, following Eq. (8). This causes a larger final abundance for the DM number density since $X' \propto \epsilon_{\Delta\chi}$. Naturally, one requires a lighter DM to satisfy the observed abundance, since $\Omega_\chi \propto m_\chi X$. As a result, the parameter space shifts towards larger DM mass as we decrease y_χ . It is possible to have DM of mass $\sim \mathcal{O}(\text{MeV})$ but at the expense of making the Yukawa couplings $y_{\chi,\phi}$ larger. Thus, inflaton decay can give rise to DM of mass from a few MeVs up to several TeVs by tuning the Yukawa couplings within perturbative range. On the right panel we see only those points which satisfy both the relic abundance and the baryon asymmetry in the same two dimensional plane of $y_\chi - m_\chi$ as in the left, but now the colour coding is done with respect to y_ϕ . As we have already seen, a

smaller y_χ requires a larger DM mass to satisfy the relic abundance, here we see for such points, in order to satisfy the observed η_B , a larger y_φ is needed as well. Since a small y_χ implies a larger branching $\text{Br} \propto y_\chi/(y_\chi + y_N)$ of the RHN into the SM final states, resulting a larger asymmetry in the visible sector, hence one needs to have a smaller y_φ to reduce the RHN yield. This will automatically result in a decrement of \tilde{N}_{B-L} as $\tilde{N}'_{B-L} \propto \tilde{\rho}_N \propto \Gamma_\varphi$. Thus, a larger y_χ requires a smaller y_φ and a larger m_χ to satisfy both the relic density and the right baryon asymmetry.

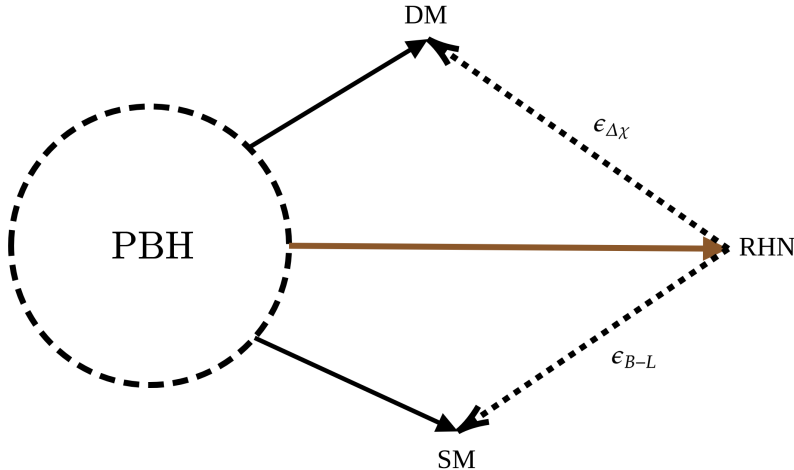


Figure 8. Schematic diagram of asymmetry production in the dark and in the visible sector in presence of primordial black holes.

IV. ASYMMETRIC DARK MATTER FROM PBH EVAPORATION

So far we have discussed the generation of asymmetries from the decay of inflaton in a model-agnostic way. In this section we will consider a scenario where asymmetries can emerge from the decay of the primordial black holes⁶. To be more specific, the asymmetries result from out-of-equilibrium decay of RHN with the dominant contribution coming from non-thermal RHNs produced from the evaporation of PBH. However, the situation is a bit different here as unlike in the case of inflation where inflaton coupling could be tuned in

⁶A recent review of PBH may be found in [78].

a way such that it decays only into RHN, PBH, on the other hand, can emit *all* particles democratically. The scenario is schematically shown in Fig. 8. We discuss the interesting features of PBH briefly below followed by detailed discussion of its role in creation of asymmetries in dark as well as visible sectors.

A. Primordial Black Hole: formation and constraints

We assume PBHs are formed after inflation during the era of radiation domination. Assuming radiation domination, the mass of the black hole from gravitational collapse is typically close to the value enclosed by the post-inflation particle horizon and is given by [79, 80]

$$m_{\text{BH}} = \frac{4}{3} \pi \gamma \left(\frac{1}{\mathcal{H}(T_{\text{in}})} \right)^3 \rho_{\text{rad}}(T_{\text{in}}) \quad (26)$$

with

$$\rho_{\text{rad}}(T_{\text{in}}) = \frac{3}{8\pi} \mathcal{H}(T_{\text{in}})^2 M_{\text{pl}}^2 \quad (27)$$

and $\gamma \simeq 0.2$ is a numerical factor which contains the uncertainty of the PBH formation. As mentioned earlier, PBHs are produced during the radiation dominated epoch, when the SM plasma has a temperature $T = T_{\text{in}}$ which is given by

$$T_{\text{in}} = \left(\frac{45 \gamma^2}{16 \pi^3 g_{\star}(T_{\text{in}})} \right)^{1/4} \sqrt{\frac{M_{\text{pl}}}{m_{\text{BH}}(T_{\text{in}})}} M_{\text{pl}}. \quad (28)$$

Once formed, PBH can evaporate by emitting Hawking radiation [81, 82]. A PBH can evaporate efficiently into particles lighter than its instantaneous temperature T_{BH} defined as [82]

$$T_{\text{BH}} = \frac{1}{8\pi G m_{\text{BH}}} \approx 1.06 \left(\frac{10^{13} \text{ g}}{m_{\text{BH}}} \right) \text{ GeV}, \quad (29)$$

where G is the universal gravitational constant. The mass loss rate can be parametrised as [83]

$$\frac{dm_{\text{BH}}(t)}{dt} = -\frac{\mathcal{G} g_{\star}(T_{\text{BH}})}{30720 \pi} \frac{M_{\text{pl}}^4}{m_{\text{in}}(t)^2}, \quad (30)$$

where $\mathcal{G} \sim 4$ is the grey-body factor. Here we ignore the temperature dependence of g_* during PBH evolution, valid in the pre-sphaleron era. On integrating Eq. (30) we end up with the PBH mass evolution equation as

$$m_{\text{BH}}(t) = m_{\text{in}}(T_{\text{in}}) \left(1 - \frac{t - t_{\text{in}}}{\tau}\right)^{1/3}, \quad (31)$$

with

$$\tau = \frac{10240 \pi m_{\text{in}}^3}{\mathcal{G} g_*(T_{\text{BH}}) M_{\text{pl}}^4}, \quad (32)$$

as the PBH lifetime. Here onward we will use $m_{\text{in}}(T_{\text{in}})$ simply as m_{in} . The evaporation temperature can then be computed taking into account $H(T_{\text{evap}}) \sim \frac{1}{\tau^2} \sim \rho_{\text{rad}}(T_{\text{evap}})$ as

$$T_{\text{evap}} \equiv \left(\frac{45 M_{\text{pl}}^2}{16 \pi^3 g_*(T_{\text{evap}}) \tau^2}\right)^{1/4}. \quad (33)$$

However, if the PBH component dominates at some point the total energy density of the universe, the SM temperature just after the complete evaporation of PBHs is: $\bar{T}_{\text{evap}} = 2/\sqrt{3} T_{\text{evap}}$ [84].

The initial PBH abundance is characterized by the dimensionless parameter β that is defined as

$$\beta \equiv \frac{\rho_{\text{BH}}(T_{\text{in}})}{\rho_{\text{rad}}(T_{\text{in}})}, \quad (34)$$

that corresponds to the ratio of the initial PBH energy density to the SM energy density at the time of formation. Note that, β steadily grows until PBH evaporation since the PBH energy density scales like non-relativistic matter $\sim a^{-3}$, while the radiation energy density scales as $\sim a^{-4}$. Therefore, an initially radiation-dominated universe will eventually become matter-dominated if the PBHs are still around. The condition of PBH evanescence during radiation domination can be expressed as [80]

$$\beta < \beta_{\text{crit}} \equiv \gamma^{-1/2} \sqrt{\frac{\mathcal{G} g_*(T_{\text{BH}})}{10640 \pi}} \frac{M_{\text{pl}}}{m_{\text{in}}}, \quad (35)$$

where β_c is the critical PBH abundance that leads to early matter-dominated era. Note that for simplicity, we consider a monochromatic mass function of PBHs implying all PBHs to have identical masses. Additionally, the PBHs are assumed to be of Schwarzschild type without any spin and charge. The gravitational waves (GW) induced by large-scale density perturbations laid by PBHs could lead to a backreaction problem [84, 85], that can be avoided if the energy contained in GWs never overtakes the one of the background universe or in other words if

$$\beta < 10^{-4} \left(\frac{10^9 \text{g}}{m_{\text{in}}} \right)^{1/4}. \quad (36)$$

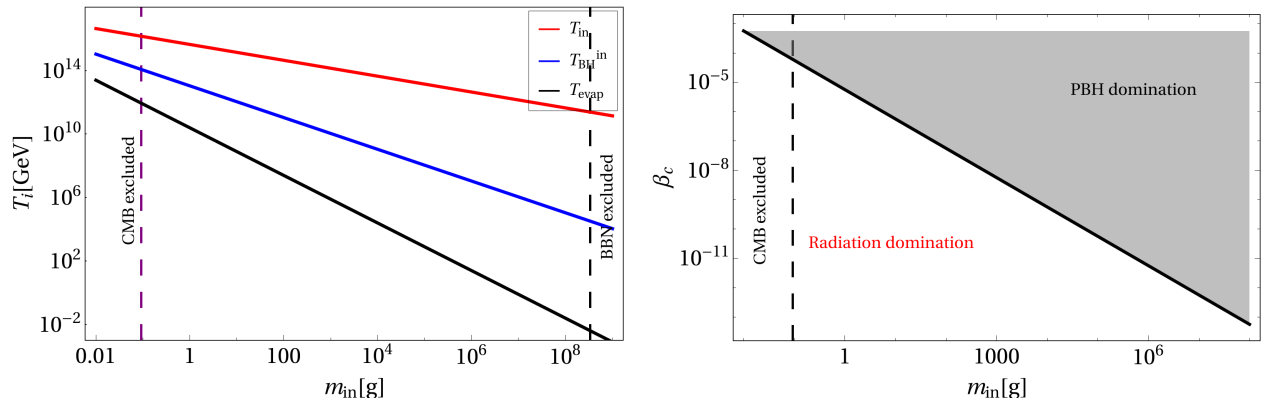


Figure 9. Left panel: PBH formation (red), evaporation (black) and the Hawking temperature (blue) as a function of the PBH mass. The purple and black dashed vertical lines correspond to the lower and upper bounds from CMB and BBN (see text). Right panel: β_c as a function of PBH mass where the black thick diagonal line segregates radiation domination vs PBH domination.

In left panel of Fig. 9 we have shown the dependence of T_{BH} , T_{in} and T_{evap} on the PBH mass. As one can see, T_{evap} falls fast with the rise in PBH mass (black solid line), while lighter PBHs have larger formation temperature. From the right panel, on the other hand, we find that in order to have PBH domination, β has to be large enough for lighter PBH. As we will see, to produce observed baryon asymmetry together with right DM abundance, we need to rely upon ultralight PBHs and a comparatively large β ensuring PBH domination. Since PBH evaporation produces all particles, including radiation that can disturb the successful predictions of BBN, hence we require $T_{\text{evap}} > T_{\text{BBN}} \simeq 4 \text{ MeV}$. This can be translated into

an upper bound on the PBH mass. On the other hand, a lower bound on PBH mass can be obtained from the CMB bound on the scale of inflation [77] : $\mathcal{H}_I \equiv \mathcal{H}(T_{\text{in}}) \leq 2.5 \times 10^{-5} M_{\text{pl}}$, where $\mathcal{H}(T_{\text{in}}) = \frac{1}{2t_{\text{in}}}$ with $t(T_{\text{in}}) = \frac{m_{\text{in}}}{M_{\text{pl}}^2 \gamma}$ (as obtained from Eq. (26)). Using these BBN and CMB bounds together, we have a window for allowed initial mass for PBH that reads

$$0.1 \text{ g} \lesssim m_{\text{in}} \lesssim 3.4 \times 10^8 \text{ g} . \quad (37)$$

The range of PBH masses between these bounds is at present generically unconstrained [78]. While PBH can evaporate by Hawking radiation, it can be stable on cosmological scales if sufficiently heavy, potentially giving rise to some or all of DM [86]. The bounds and signatures of such heavy PBHs can be very different from the ones mentioned above and we do not discuss such cosmologically long-lived PBH any further.

B. Right handed neutrino from PBH: Dark Matter and Baryogenesis

Initially proposed by Hawking [81, 82], PBH can have several interesting consequences in cosmology [87, 88]. Even though the light PBHs of our interest are not long lived enough to be DM, they can still play non-trivial roles in genesis of DM as well as baryogenesis. Since PBH evaporate to all particles, irrespective of their SM gauge interactions, it can lead to production of DM, leptons, baryons etc as well as other heavy particles like RHN in our model. Although the evaporation of PBH in such a minimal scenario can not produce dark or visible sector asymmetries⁷ on its own, it can produce heavy particles like RHNs whose subsequent decay can produce the required asymmetries. Such a role of PBH evaporation on baryogenesis was first pointed out in [81, 88] followed by some detailed study in [90] and recently it has been taken up by several authors in different contexts [68, 79, 91–96]⁸. On the other hand, the role of PBH evaporation on DM genesis have been studied for different DM scenarios [84, 93, 98–100]. Thus, PBH evaporation can lead to the generation of both RHNs and DM, depending on the PBH mass (see, for example, [68, 79, 80, 93, 94, 96, 99–103]). However, in the present framework, we are not interested in DM generation from direct PBH

⁷One can also generate a chemical potential directly from PBH evaporation, as discussed within the framework of gravitational baryogenesis [89].

⁸In [97], the authors found that the rate of baryon number violation via sphaleron transitions in the standard model can be enhanced in the presence of PBH.

evaporation, rather we are interested in the scenario of DM production from the asymmetry generated in the dark sector via RHN decay. While we can not prevent DM generation from PBH evaporation, eventually DM abundance is dictated by its asymmetric component only, which is generated by the RHN decay only.

Before doing the complete numerical analysis, we first show the key features of such a scenario by using approximate analytical expressions. The total number of RHNs \mathcal{N} with mass M_N emitted during PBH evaporation can be estimated using [90, 102]

$$d\mathcal{N} = -\frac{d(m_{\text{in}})}{3T_{\text{BH}}^{\text{in}}}, \quad (38)$$

which gives rise to

$$\mathcal{N} = \frac{g_{\mathcal{N}}}{g_{\star}(T_{\text{BH}})} \begin{cases} \frac{4\pi}{3} \left(\frac{m_{\text{in}}}{M_{\text{pl}}}\right)^2 & \text{for } M_N < T_{\text{BH}}^{\text{in}}, \\ \frac{1}{48\pi} \left(\frac{M_{\text{pl}}}{M_N}\right)^2 & \text{for } M_N > T_{\text{BH}}^{\text{in}}, \end{cases} \quad (39)$$

where $g_{\mathcal{N}}$ is the number of degrees of freedom for the RHN and $T_{\text{BH}}^{\text{in}} = T_{\text{BH}}(t = t_{\text{in}})$ is the initial PBH temperature. Note that, for $M_N < T_{\text{BH}}^{\text{in}}$, PBH emits RHNs from the beginning, namely the formation of PBHs. In the opposite case, PBH emits RHNs only after its Hawking temperature reaches M_N .

The PBHs emit RHNs (along with all the SM particles and DM), and the CP-violating decays of such non-thermal RHNs produce the lepton asymmetry. This lepton asymmetry is then further converted into the observed baryon asymmetry via sphaleron transition like in standard leptogenesis scenario. If \mathcal{N} is the number of RHNs emitted from a single PBH then the present baryon number yield can be written as [79, 90, 96]

$$\frac{n_B}{s}(T_0) = \mathcal{N} \epsilon_1 a_{\text{sph}} \frac{n_{\text{PBH}}}{s} \Big|_{T_{\text{evap}}}, \quad (40)$$

where we assume no further entropy production after PBH evaporation.

It is possible to analytically derive the mass range of RHNs emitted from PBH evaporation that can provide the required lepton asymmetry. In the Type-I seesaw mechanism, the quantity ϵ has an upper bound [41, 59]

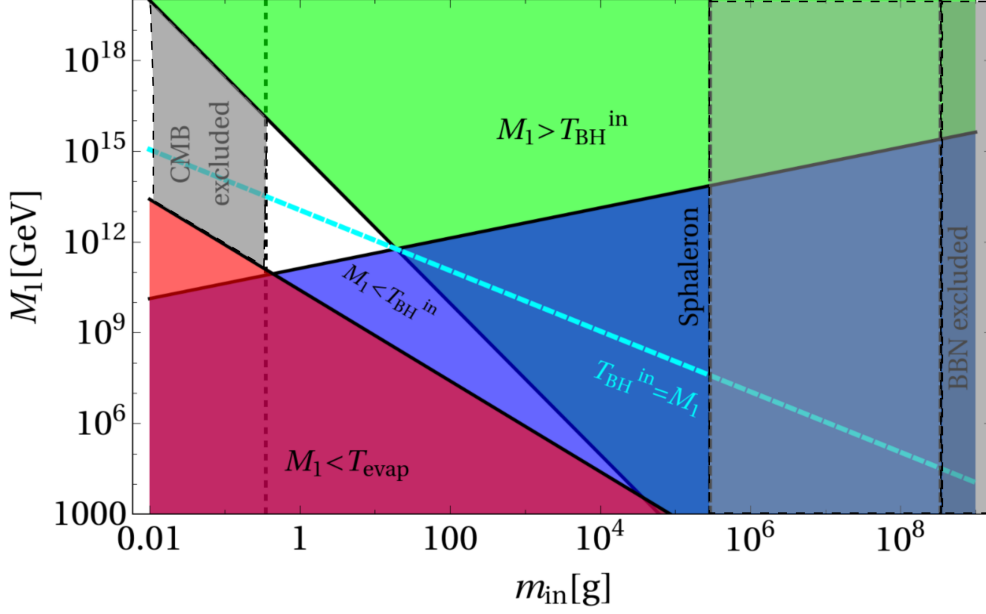


Figure 10. Bound on RHN mass from the requirement of obtaining observed baryon asymmetry from PBH evaporation. All the coloured regions are discarded from the bounds derived in Eq. (42) and Eq. (44). The vertical black dashed line corresponds to (from left to right) the bound from the scale of inflation (CMB), sphaleron transition and BBN. The white triangular region in the middle is the region that is allowed.

$$\epsilon \lesssim \frac{3}{16\pi} \frac{M_1 m_{\nu, \max}}{v^2}, \quad (41)$$

where $v = 246$ GeV is the SM Higgs VEV and $m_{\nu, \max}$ is the mass of the heaviest light neutrino. On the other hand, the final asymmetry produced from PBH evaporation as computed from Eq. (40), $Y_B = n_B/s \Big|_{T_0} \simeq 8.7 \times 10^{-4}$ [77]. These together constrain the mass of the RHN produced from PBH evaporation both from above and from below

$$M_1 \begin{cases} > \frac{2g_*(T_{\text{BH}})}{a_{\text{sph}} g_N} \frac{M_{\text{pl}}^2 v^2}{m_{\nu, \max} m_{\text{in}}^2} Y_B(T_0) \frac{n_{\text{PBH}}}{s} \Big|_{T_{\text{evap}}} & \text{for } M_1 < T_{\text{BH}}^{\text{in}}; \\ < \frac{a_{\text{sph}} g_N}{128\pi g_*(T_{\text{BH}})} \frac{M_{\text{pl}}^2 m_{\nu, \max}}{v^2} \frac{1}{Y_B(T_0)} \frac{n_{\text{PBH}}}{s} \Big|_{T_{\text{evap}}} & \text{for } M_1 > T_{\text{BH}}^{\text{in}}, \end{cases} \quad (42)$$

where we have used

$$n_{\text{PBH}}(T_{\text{evap}}) = \frac{1}{m_{\text{in}}} \frac{\pi^2}{30} g_{\star}(T_{\text{evap}}) T_{\text{evap}}^4. \quad (43)$$

Another bound comes from the fact that if $M_1 < T_{\text{evap}}$, then the RHNs produced from PBH evaporation are in thermal bath and then washout processes are in effect. Hence, to ensure non-thermal production of baryon asymmetry one must follow [79]

$$M_1 > T_{\text{evap}} \implies M_1 \gtrsim 3 \times 10^{-3} \left(\frac{\mathcal{G}^2 g_{\star}(T_{\text{evap}}) M_{\text{pl}}^{10}}{m_{\text{in}}^6} \right)^{1/4}. \quad (44)$$

For scenarios where both thermal and non-thermal RHNs were taken into account for generation of lepton asymmetry, one may refer to [68, 95].

Lastly, in order for lepton asymmetry to be sufficiently generated from RHNs produced from PBH evaporation, one requires evaporation to be over before sphaleron transition $T_{\text{evap}} \gtrsim T_{\text{EW}}$, which translates into the corresponding bound on initial PBH mass

$$m_{\text{in}} \lesssim 3 \times 10^5 \text{ g}. \quad (45)$$

However, this bound similar to the BBN bound is naturally satisfied as one can see from Fig. 10. We thus find that the observed baryon asymmetry is produced over a very tiny region for $10^{11} \lesssim M_1 \lesssim 10^{16}$ GeV and $0.5 \lesssim m_{\text{in}} \lesssim 10$ g, depicted by the white triangular region in Fig. 10.

While the PBH evaporation can not create baryon asymmetry directly in our minimal scenario, it can create DM directly, as discussed in different contexts [80, 84, 93, 98, 101, 104–119]. However, in asymmetric DM scenario, the final DM abundance is dictated by the dark sector asymmetry which is created only by the out-of-equilibrium decay of RHN where the latter is produced dominantly from PBH evaporation. Thus, in the present scenario asymmetric DM yield can be expressed as

$$Y_{\text{DM}}(T_0) = \epsilon_{\Delta\chi} \mathcal{N} \frac{n_{\text{PBH}}}{s}(T_{\text{evap}}), \quad (46)$$

that leads to DM abundance

$$\Omega_{\text{DM}} h^2 = \frac{m_{\text{DM}} s_0}{\rho_c} Y_{\text{DM}}(T_0), \quad (47)$$

where \mathcal{N} is defined via Eq. (39), which results is

$$\Omega_{\text{DM}} h^2 = \frac{g_{\text{DM}}}{g_\star(T_{\text{evap}})} \frac{m_{\text{DM}} s_0}{\rho_c} \epsilon_{\Delta\chi} \frac{n_{\text{PBH}}}{s} \Big|_{T_{\text{evap}}} \begin{cases} \frac{4\pi}{3} (m_{\text{in}}/M_{\text{pl}})^2 & \text{for } T_{\text{BH}}^{\text{in}} > M_1; \\ \frac{1}{48\pi} (M_{\text{pl}}/M_1)^2 & \text{for } T_{\text{BH}}^{\text{in}} < M_1. \end{cases} \quad (48)$$

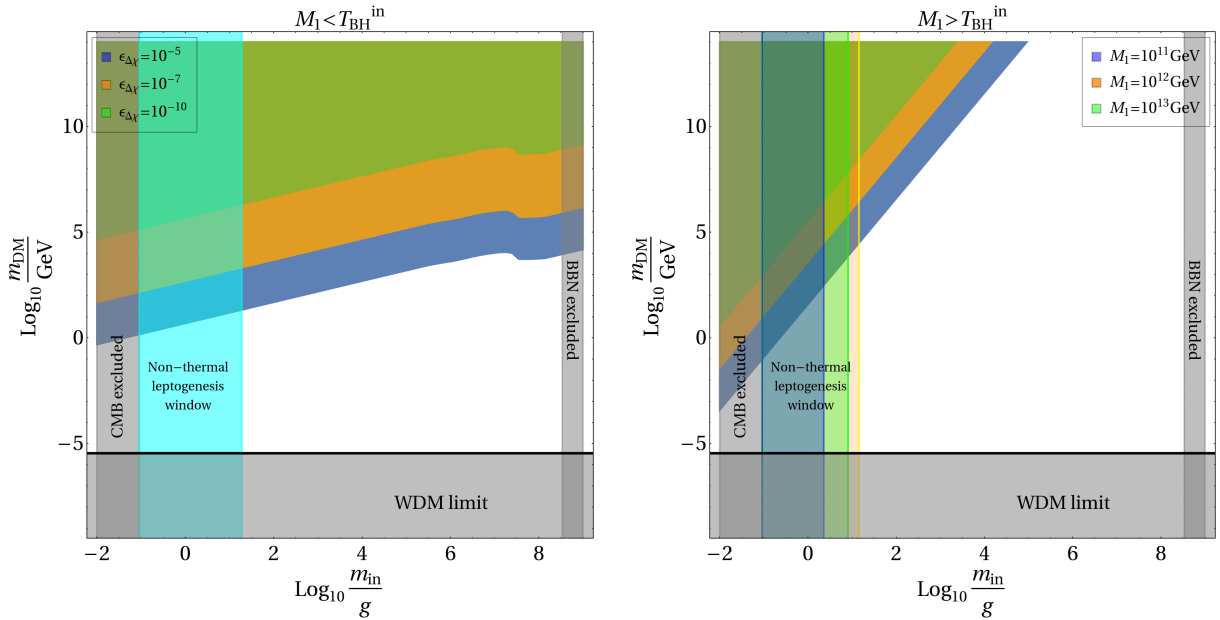


Figure 11. The dark green, orange and blue coloured regions are excluded from DM overproduction due to different choices of DM asymmetry (left panel) and RHN mass (right panel) shown by different colours. In the right panel we have chosen $\epsilon_{\Delta\chi} = 10^{-10}$. The gray shaded regions are disallowed from CMB, BBN and warm DM limit, while the cyan band (left) is where non-thermal leptogenesis from PBH is allowed for $M_1 \simeq 10^{12}$ GeV (see text).

Note that the final DM asymmetry depends on the mass of RHN as expected. To match the observed DM abundance $\Omega_{\text{DM}} h^2 \simeq 0.12$, the DM yield has to be fixed so that $m_{\text{DM}} Y_0 = \Omega_{\text{DM}} h^2 \frac{1}{s_0} \frac{\rho_c}{h^2} \simeq 4.3 \times 10^{-10}$ GeV, where $\rho_c \simeq 1.1 \times 10^{-5} h^2$ GeV/cm³ is the critical energy density and $s_0 \simeq 2.9 \times 10^3$ cm⁻³ is the entropy density at present [5]. Fig. 11 depicts the allowed mass range for the DM obtained analytically using Eq. (48). In the left panel, different regions shown by the green, orange and blue colours correspond to different choices

of DM asymmetry $\epsilon_{\Delta\chi}$, for the case where $T_{\text{BH}}^{\text{in}} > M_1$. All these regions correspond to DM overabundance and hence discarded. Here we see larger asymmetry imposes tighter constraint on the DM mass. This is expected since a larger asymmetry results in larger asymmetric DM abundance as per Eq. (48). Hence slight increase in the DM mass results in overabundance. The slight distortion in the large DM mass region is due to the change in the number of light degrees of freedom around $T_{\text{evap}} \simeq 150$ MeV, i.e., around the time of QCD phase transition. In the opposite limit $T_{\text{BH}}^{\text{in}} < M_1$, shown in the right panel, we see a lighter RHN imposes tighter bound since $\Omega_{\text{DM}} \propto 1/M_1^2$ for a fixed CP asymmetry $\epsilon_{\Delta\chi} = 10^{-10}$.

In order not to spoil the structure formation, a fermion DM candidate which is part of the thermal bath or produced from the thermal bath should have mass above a few keV in order to give required free-streaming of DM as constrained from Lyman- α flux-power spectra [120–122]. Such light DM of keV scale leads to a warm dark matter (WDM) scenario having free-streaming length within that of cold and hot DM. If such light DM is also produced from PBH evaporation, it leads to a potential hot component in total DM abundance, tightly constrained by observations related to the CMB and baryon acoustic oscillation (BAO) leading to an upper bound on the fraction of this hot component with respect to the total DM, depending on the value of DM mass [123]. A conservative 10 % upper bound on such hot dark matter (HDM) component [84] can lead to similar constraints on DM mass along with PBH initial fraction. The requirement of producing right relic abundance, together with these lower limits on the DM mass put tight constraint on the DM mass emitted by the PBH. This is shown by the gray shaded regions in Fig. 11. We also show the window of PBH mass in cyan where successful non-thermal leptogenesis from RHN emitted by PBH is possible (Fig. 10) for $M_1 \simeq 10^{12}$ GeV. In the right panel we have chosen different masses for the RHN, corresponding to which the allowed mass window for non-thermal leptogenesis changes (maximum for $M_1 = 10^{12}$ GeV shown in orange) as denoted by different coloured vertical bands. The upshot of Fig. 11 is that, it is possible to generate observed asymmetry in visible sector, together with right relic abundance of asymmetric DM with ultralight PBH and for DM mass $\gtrsim 10^{-5}$ GeV. The upper bound on the DM mass depends on the size of the asymmetry generated within the dark sector, which depends also on the RHN mass scale. Finally, it is also importance to note that a large initial abundance of PBHs increases the DM capture rate and makes the DM under-abundant. However, this is found to be significant

only for superheavy DM with mass $\sim 10^8$ GeV (for fermion) and $\beta \gtrsim 10^{-4}$ [84, 98].

C. Results and Discussions

In order to compute the asymmetries we will now perform a full numerical analysis considering a set of coupled BEQs accounting for the energy and number densities of different components. We focus on the production of the observed baryon asymmetry via non-thermal leptogenesis, together with the correct relic abundance for the asymmetric DM. Thus, we track the evolution of the comoving number densities of the RHN, PBH, lepton and DM asymmetries and the radiation energy density via their coupled BEQs. What is crucial here is the fact that since the PBHs are assumed to be produced during the radiation dominated era, hence thermal contribution to leptogenesis can not be overlooked. The evolution equation for PBH mass, energy densities and bath temperature⁹ in presence of PBH reads [68, 95]

$$\begin{aligned}
\frac{dm_{\text{BH}}}{d\xi} &= -\frac{\kappa}{\xi \mathcal{H}} \epsilon(m_{\text{BH}}) \left(\frac{1g}{m_{\text{BH}}} \right)^2, \\
\frac{d\tilde{\rho}_R}{d\xi} &= -\frac{\epsilon_{\text{SM}}(m_{\text{BH}})}{\epsilon(m_{\text{BH}})} \frac{\xi}{m_{\text{BH}}} \frac{dm_{\text{BH}}}{d\xi} \tilde{\rho}_{\text{BH}}, \\
\frac{d\tilde{\rho}_{\text{BH}}}{d\xi} &= \frac{1}{m_{\text{BH}}} \frac{dm_{\text{BH}}}{d\xi} \tilde{\rho}_{\text{BH}}, \\
\frac{dT}{d\xi} &= -\frac{T}{\Delta} \left[\frac{1}{\xi} + \frac{\epsilon_{\text{SM}}(m_{\text{BH}})}{\epsilon(m_{\text{BH}})} \frac{1}{m_{\text{BH}}} \frac{dm_{\text{BH}}}{d\xi} \frac{g_{\star}(T)}{g_{\star s}(T)} \xi \frac{\tilde{\rho}_{\text{BH}}}{4\tilde{\rho}_R} \right],
\end{aligned} \tag{49}$$

where

$$\Delta = 1 + \frac{T}{3g_{\star s}(T)} \frac{dg_{\star s}(T)}{dT}, \tag{50}$$

takes care of the variation of the total number of DOFs with temperature and $\xi = a/a_I$ (with $a_I = 1$) as defined earlier. The evaporation function $\epsilon(m_{\text{in}})$ is taken from [83, 102]. The coupled BEQs for the evolution of the RHN number density, DM and lepton asymmetries, on the other hand, are given by [68, 95]

⁹In principle, the BEQ for radiation should also contain the contribution from RHN decay into the thermal, but such contributions are negligible compared to the PBH contribution and can be ignored.

$$\begin{aligned}
a\mathcal{H}\frac{d\tilde{n}_{N_1}^T}{d\xi} &= -(\tilde{n}_{N_1}^T - \tilde{n}_{N_1}^{\text{eq}}) \Gamma_{N_1}^T, \\
a\mathcal{H}\frac{d\tilde{n}_{N_1}^{\text{BH}}}{d\xi} &= -\tilde{n}_{N_1}^{\text{BH}} \Gamma_{N_1}^{\text{BH}} + \Gamma_{\text{BH}\rightarrow N_1} \frac{\tilde{\rho}_{\text{BH}}}{m_{\text{in}}}, \\
a\mathcal{H}\frac{d\tilde{N}_{B-L}}{d\xi} &= \epsilon_{\Delta L} \left[(\tilde{n}_{N_1}^T - \tilde{n}_{N_1}^{\text{eq}}) \Gamma_{N_1}^T + \tilde{n}_{N_1}^{\text{BH}} \Gamma_{N_1}^{\text{BH}} \right] - \text{Br}_{\text{SM}} \mathcal{W} \tilde{N}_{B-L}, \\
a\mathcal{H}\frac{dX}{d\xi} &= \epsilon_{\Delta X} \left[(\tilde{n}_{N_1}^T - \tilde{n}_{N_1}^{\text{eq}}) \Gamma_{N_1}^T + \tilde{n}_{N_1}^{\text{BH}} \Gamma_{N_1}^{\text{BH}} \right] - \text{Br}_{\text{DM}} \mathcal{W} X,
\end{aligned} \tag{51}$$

where all \tilde{n}_{N_1} 's are comoving number densities of N_1 produced from the bath (denoted by superscript T) and PBH (denoted by superscript BH) and Br stands for the branching ratio of RHN into leptons (denoted by subscript SM) and DM (denoted by subscript DM). Similarly \tilde{N}_{B-L}, X are comoving densities of $B-L$ and dark sector asymmetries respectively. The thermally averaged decay rate of N_1 is denoted by $\Gamma_{N_1}^T$ and $\tilde{n}_{N_1}^{\text{eq}}$ is the equilibrium number density. The Hubble parameter \mathcal{H} entering in the Boltzmann equations is given by

$$\mathcal{H} = \sqrt{\frac{8\pi}{3M_{\text{pl}}^2} \frac{\tilde{\rho}_{\text{BH}} a_I \xi + \tilde{\rho}_R}{a_I^4 \xi^4}}, \tag{52}$$

and $\Gamma_{\text{BH}\rightarrow N_1}$ is the non-thermal production term for N_1 (originating from PBH evaporation) and can be written as [95, 102]

$$\Gamma_{\text{BH}\rightarrow N_1} = \int_0^\infty \frac{d^2 \mathcal{N}}{dp dt} dp \simeq \frac{27 T_{\text{BH}}}{32 \pi^2} (-z_{\text{BH}} \text{Li}_2(-e^{-z_{\text{BH}}}) - \text{Li}_3(-e^{-z_{\text{BH}}})) , \tag{53}$$

where $\text{Li}_s(z)$ are the poly-logarithm functions of order s and $z_{\text{BH}} = M_1/T_{\text{BH}}$. Γ_1^{BH} is the decay width corrected by an average time dilation factor [95]

$$\Gamma_{N_1}^{\text{BH}} = \left\langle \frac{M_1}{E_1} \right\rangle_{\text{BH}} \Gamma_1 \approx \frac{K_1(M_1/T_{\text{BH}})}{K_2(M_1/T_{\text{BH}})} \Gamma_1, \tag{54}$$

where $K_{1,2}[\dots]$ are the modified Bessel functions of second kind and the thermal average is obtained assuming that the Hawking spectrum has a Maxwell-Boltzmann form, while Γ_1 is the RHN decay width given by Eq. (9). Finally, the washout factor \mathcal{W} reads [70]

$$\mathcal{W} = \frac{1}{4} \Gamma_{N_1}^T K_2(z) z^2, \tag{55}$$

where $z \equiv M_1/T$ and we are ignoring the flavour effects as well as the scattering processes leading to washouts. The generation of lepton asymmetry has thermal and non-thermal sources stemming from the plasma and PBH evanescence respectively. On the other hand, DM can be present in the thermal bath while its asymmetric component arises from RHN decay and eventually only the asymmetric component survives. From Fig. 10 we have already realized that non-thermal leptogenesis from PBH necessarily requires ultralight PBH with $M_1 \gtrsim 10^{12}$ GeV. On the other hand, it is clear from the right panel of Fig. 9, for very light PBHs to dominate the energy density, the initial energy fraction of PBH density should be much higher. Hence, a long period of PBH domination is preferred for purely non-thermal leptogenesis from PBH [96]. Otherwise, the asymmetry production will be dominated by thermally generated RHNs with PBH leading to subsequent entropy dilution only [68, 95]. For N_2 leptogenesis, one can as well get an enhancement of asymmetry in the presence of PBH compared to the usual thermal case [68]. However, we restrict ourselves to N_1 leptogenesis only and consider the production to be dominant from non-thermal RHNs produced from PBH evaporation. In the rest of the analysis we will thus restrict the RHN mass to be $M_1 = 10^{12}$ GeV unless otherwise specified. We will first look at the impact of having PBHs on the energy densities and the yield of the asymmetries in visible and dark sectors. For this we consider some benchmark masses of the PBH in 1-100 g range falling in the allowed region of Fig. 10. We also fix the N_1 -DM Yukawa coupling $y_\chi = 0.1$ that determines the asymmetry in dark sector.

The top left panel of Fig. 12 shows the evolution of radiation (orange) and PBH (black) energy densities with scale factor for PBH mass of 1 g. Here we see with time the PBH energy density rises compared to that of radiation (as $\rho_{\text{BH}} \sim a^{-3}$) and at around $\xi \sim 10^3$ the PBH energy density overtakes the radiation density. This corresponds to a bath temperature $T \sim 10^{12}$ GeV that can be read off from the adjacent panel on the right. Slightly beyond this point, the energy density in PBH shows a plateau. This plateau region gets broadened as the PBH mass increases (middle and bottom left panels) since a larger mass corresponds to a smaller evaporation temperature (Eq. (33)). As a result, for ultralight masses, PBH domination era gets over earlier. The PBH dominated era ends¹⁰ at $\xi \sim 10^6$ for upper left panel plot where we see the black curve falls sharply. As the PBH evaporation dumps

¹⁰PBH evaporation process, which is effectively instantaneous in sudden reheating approximation, transforms large density fluctuations into radiation and yields large pressure waves [124, 125].

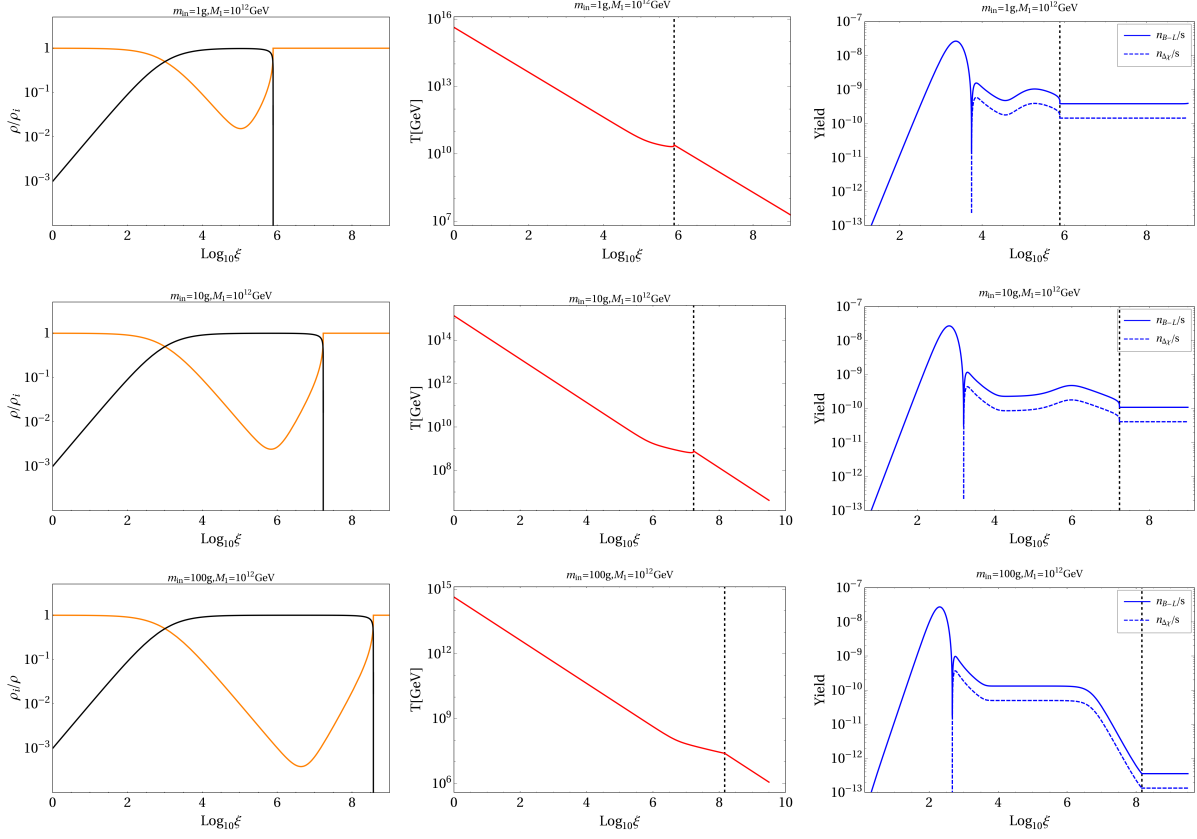


Figure 12. Energy density (left column), temperature of thermal bath (middle column) and yield of asymmetries (right column) as a function of scale factor for a three different choices of PBH mass and for a fixed RHN mass as mentioned in the plot label. In all cases we have considered PBH domination by considering $\beta = 10^{-3}$, $M_1 = 10^{12}$ GeV and $y_\chi = 10^{-1}$. The black dashed vertical line in each case denotes the PBH evaporation time.

a huge amount of entropy into the thermal plasma, the plasma temperature shows a rise as one can notice from the kink in the red curve of upper middle panel plot. As the PBH mass increases, evaporation takes place at a later epoch, hence the kink in the red curve also shifts to a smaller temperatures as one can see from the lower middle panel plots. Plots shown in extreme right columns of Fig. 12 depict the evolution of yield of the asymmetries. The asymmetries in both the sectors evolve identically because of the same source. The asymmetries first increase because of the thermal contribution, and then diminish for the washout effect due to the inverse decay of thermal RHNs. Afterwards, they remain unchanged till the time the production of non-thermal RHN from PBH overtakes the

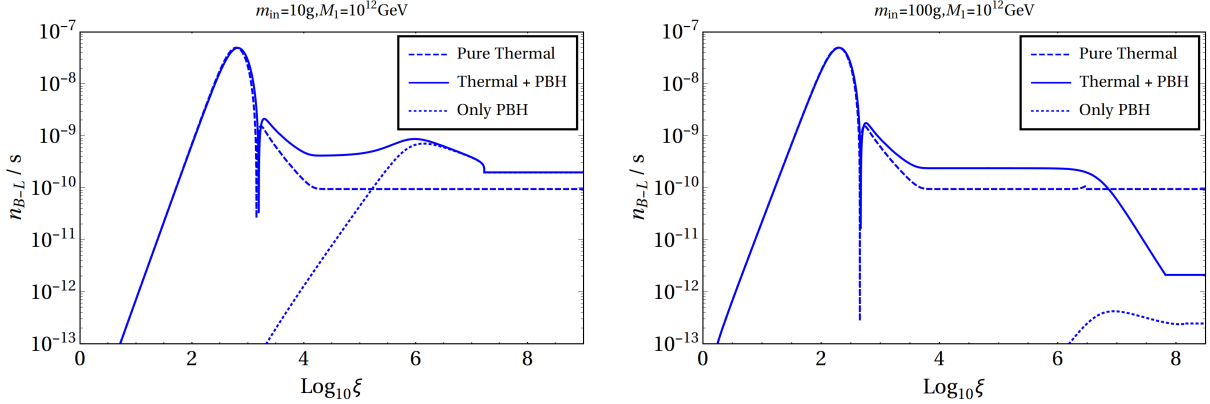


Figure 13. Evolution of the yield of asymmetries for three scenarios : (i) purely thermal, (ii) only non-thermal contribution from PBH and (iii) both thermal as well as non-thermal contributions. Here, $\beta = 10^{-3}$, $M_1 = 10^{12}$ GeV and $y_\chi = 10^{-1}$. The left panel represents a lighter PBH mass of 10 g, whereas the right panel shows the evolution for a higher PBH mass of 100 g.

thermal contribution. Then during the period of PBH evaporation dilution effect becomes significant (depending on the PBH mass) because of entropy injection in the thermal bath. Finally, the asymmetries saturate once the PBH is completely evaporated. The effect of entropy injection becomes more prominent for comparatively massive PBH as the period of evaporation becomes longer. For better understanding of the asymmetry evolution, in Fig. 13, we compare three scenarios where the baryon asymmetry results from the decay of (i) only thermal RHN (dashed line) in the absence of PBH, (ii) only non-thermal RHN produced from PBH (dotted line) and (iii) both thermal as well as non-thermal RHN (solid line) for two different PBH masses. These plots clearly show the difference in the yield of baryon asymmetry for these three cases. For the lighter PBH mass as shown in the left panel of Fig. 13, one finds that even after the entropy injection due to the PBH evaporation, the final baryon asymmetry remains larger than the one obtained in the scenario with no PBH¹¹. On the other hand, for a heavier PBH as shown in the right panel of Fig. 13, one expects a relatively larger entropy injection resulting in a larger dilution of the final baryon asymmetry, making it lesser in comparison to the one produced in thermal leptogenesis. Since asymmetries in dark and visible sectors evolve similarly, one can also expect that for

¹¹For comparatively lighter RHN, the effect of PBH on the final asymmetry is negligible [96], however to ensure non-thermal production we stick to $M_1 \gtrsim 10^{11}$ GeV following Fig. 10.

lighter PBH masses, the asymmetric DM production will be more compared to a purely thermal scenario discussed in earlier works.

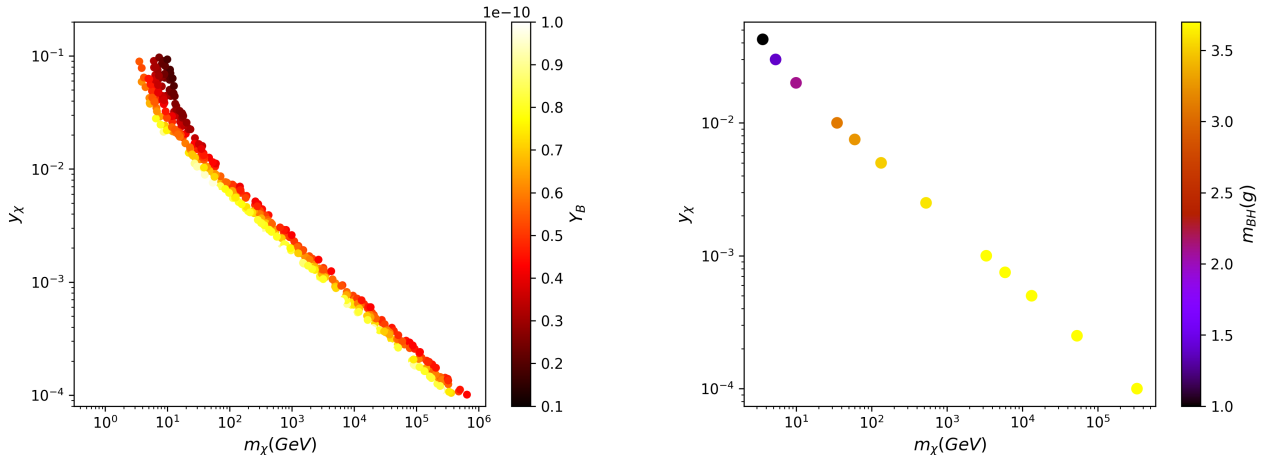


Figure 14. Left panel: Parameter space satisfying observed DM abundance in the bi-dimensional plane of $y_\chi - m_\chi$, where the colour coding is done with respect to Y_B . Right panel: Points satisfying both observed relic abundance and baryon asymmetry in $y_\chi - m_\chi$ plane, where the colour code shows variation of PBH mass. We have considered $\beta = 8 \times 10^{-3}$ to ensure PBH domination.

In Fig. 14 we have illustrated the viable parameter space where asymmetric DM relic abundance and observed baryon asymmetry can be produced entirely from RHNs emitted due to PBH evaporation by solving the set of BEQs numerically. We have performed a scan over the following parameters

$$m_\chi : \{1 - 10^5\} \text{ GeV}; m_{\text{BH}} : \{1 - 12\} \text{ g}; y_\chi : \{10^{-4} - 10^{-1}\}, \quad (56)$$

by keeping $M_1 = 10^{12} = M_2/50$ GeV and $\beta = 8 \times 10^{-3}$ to be fixed to ensure PBH domination as discussed before. The Dirac Yukawa coupling of neutrinos get fixed via Casas-Ibarra parametrisation mentioned earlier, after using the best-fit values of light neutrino parameters [6]. In the left panel of Fig. 14, we show the allowed parameter space giving correct ADM abundance in $y_\chi - m_\chi$ plane while the colour code denotes the baryon asymmetry generated. As can be seen from this plot, for heavier DM mass, one requires smaller Yukawa coupling y_χ . This is because heavier DM requires smaller dark asymmetry $\epsilon_{\Delta\chi}$ and hence smaller y_χ to generate correct relic abundance, following Eq. (48). The parameter space gets broadened

as the PBH mass keeps varying. The right panel shows, to satisfy the right ADM relic along with observed baryon asymmetry via non-thermal leptogenesis, one has to necessarily rely on ultralight PBH which we have already realized from Fig. 10 and 11. The fact that heavier PBH mass requires heavier DM mass and hence smaller Yukawa y_χ to get smaller $\epsilon_{\Delta\chi}$, can also be understood from Fig. 11 based on approximate analysis. The results of complete numerical analysis also matches with this pattern as seen from the right panel plot of Fig. 14.

V. POSSIBLE UV COMPLETION OF THE DARK SECTOR

In the minimal setup discussed above, we have considered the dark sector to be composed of a Dirac fermion χ and a singlet scalar assuming them to be odd under a \mathbb{Z}_2 symmetry. The singlet scalar, being heavier than DM χ , can decay into DM and SM particles. Thus, the only renormalisable interaction of DM χ is via RHN portal. The same RHN decays eventually produce the asymmetry in dark sector. Since the final relic abundance of DM is dictated by the asymmetric component only, it is important to make sure that the symmetric part annihilates away sufficiently in the early universe. This demands some new interactions of the DM as the RHN portal interaction is not strong enough to ensure that, specially when both RHN and the singlet scalar are both heavier compared to DM.

The simplest UV completion for dark sector is a dark Abelian gauge symmetry $U(1)_D$ under which DM χ and the singlet scalar \mathcal{S} have equal and opposite charges, assumed to be ± 1 for simplicity. The relevant dark sector Lagrangian can be written as

$$\mathcal{L}_{\text{DM}} \supset i \bar{\chi} \gamma^\mu D_\mu \chi + \frac{\epsilon}{2} B^{\alpha\beta} Y_{\alpha\beta}, \quad (57)$$

where $D_\mu = \partial_\mu + ig_D Z'_\mu$ is the covariant derivative and $B^{\alpha\beta}, Y_{\alpha\beta}$ are the field strength tensors of $U(1)_D, U(1)_Y$ respectively with ϵ being the kinetic mixing between them. Since the singlet scalar can have sizeable quartic interactions with SM Higgs, it can be produced in equilibrium, and can also bring DM into equilibrium with the SM bath for the choices of Yukawa couplings y_χ discussed before. Additionally, for sizeable kinetic mixing ($\epsilon \geq 10^{-5}$)¹², the DM can be in thermal equilibrium with the SM bath in the early universe via gauge portal interactions. Now, assuming a light Z' , DM and anti-DM can preferentially pair-

¹²For a recent review on kinetic mixing bounds see [126].

annihilate into Z' pairs with a cross-section

$$\langle\sigma v\rangle\sim\frac{\pi\alpha_D^2}{m_\chi^2}\quad(58)$$

where $\alpha_D = g_D^2/(4\pi)$. Since DM cross-section can not violate the unitarity bound [127], one gets an upper bound on its mass around 10^5 GeV so that the symmetric part can be annihilated away. One can also obtain a lower bound on ADM mass of around a few keV, from the requirement of perturbative unitarity of Yukawa couplings. We have already noticed that lighter DM requires sizeable Yukawa coupling y_χ in order to create a large asymmetry. It can be checked that for DM mass below a few keV, this Yukawa coupling will become non-perturbative. Coincidentally, this bound on DM mass is also similar to the lower bound we have in PBH scenario so that the hot DM component is restricted within 10% for large PBH initial fraction β . One can put a more conservative lower bound on such DM from the requirement that the symmetric component annihilates away before the onset of BBN, in order not to inject late time entropies due to release of Z' and their subsequent decays into light SM degrees of freedom. Therefore, DM mass of a GeV or heavier should be safe from such restrictions. While similar bounds exist in asymmetric DM scenarios in general (without inflation or PBH), here we have extended such scenarios to realise non-thermal origin of asymmetries aided by inflaton and PBH.

The $U(1)_D$ sector not only ensures the annihilation of symmetric DM part, but also lead to a stable DM candidate without requiring additional discrete symmetries, depending on the charge assignments. It also forbids the Majorana mass term of χ keeping it Dirac with a conserved quantum number. While we did not discuss the origin of Z' mass, it can be done either by spontaneous symmetry breaking or the Stueckelberg mechanism [128] without affecting rest of the discussions. Depending upon the gauge kinetic mixing, DM can also show up in direct detection experiments. In addition, for light mediator Z' , one can also realise the scenario of self-interacting dark matter (see, for example, [129, 130]) motivated from small-scale structure issues of ordinary cold DM¹³. To add to the complementarity, such dark $U(1)_D$ gauge symmetry can also lead to a first order phase transition in the early universe with observational consequences [134–140].

¹³Some recent works in the direction of self-interacting DM in $U(1)_D$ model can be found in [131–133].

VI. CONCLUSION

Asymmetric dark matter (DM) has been a well-studied framework motivated from explaining the baryon-DM coincidence problem dynamically. While the minimal frameworks to realise such possibility considers a heavy particle present in the thermal bath whose CP violating decays into visible and dark sectors generate the respective asymmetries, we consider the possibility of non-thermal origin of these asymmetries. In order to keep it minimal and also to connect to the origin of light neutrino masses, we consider the extension of Type-I seesaw model with dark sector particles [35] so that the lightest right handed neutrino can play the role of creating the dark and visible sector asymmetries. The DM is assumed to be a singlet Dirac fermion χ which couples to the right handed neutrinos (RHNs) through another scalar singlet \mathcal{S} . While the interaction of the RHNs with the SM Higgs and leptons is responsible for generating the neutrino mass via Type-I seesaw mechanism, its simultaneous decay to the visible and the dark sector generates asymmetries in both the sectors. A fraction of lepton asymmetry is converted to baryon asymmetry via sphaleron transition, while the asymmetric component of χ survives and accounts for the observed DM relic. While thermalogenesis has been discussed extensively in the literature, we consider the possibility of non-thermal RHNs by invoking the presence of additional sources. In the first attempt, we consider an inflaton field in post slow-roll stage to be the source of RHNs. The RHN subsequently decays not only to produce the dark and visible asymmetries, but leads to a brief reheating period of the universe as well. We consider the inflaton to couple only to the RHNs, while being agnostic about the details of inflaton potential and other interactions. We numerically solve a set of coupled Boltzmann equations to find the abundance of dark, visible sectors along with the reheat temperature of the universe. While a wide range of DM mass remains allowed, the RHN-DM coupling y_χ is practically a free parameter and tuned accordingly to obtain the right relic density. The RHN-SM couplings are determined from the requirement of fitting light neutrino data. We choose the mass and couplings of the inflaton and the RHNs in such a way that the non-thermal leptogenesis scenario remains valid by requiring the RHN mass to be above the reheating temperature of the universe. Thus, this scenario connects the cogenesis of dark and visible sector asymmetries to the reheat temperature of the universe as the same non-thermal RHNs produced from inflaton decay plays non-trivial role in reheating and cogenesis.

In the second scenario, we extend our prescription by considering a framework where the RHNs are sourced from evaporating primordial black holes that are produced in the radiation dominated era with a monochromatic mass spectrum. While RHNs can be produced from the thermal bath as well, we show that the asymmetries produced from non-thermal RHNs dominate over the thermal one, specially for lighter PBH masses. Keeping the parameter space within such ballpark where non-thermal leptogenesis from PBH evaporation dominates over the thermal contribution in generating the $B - L$ asymmetry, we find that the observed baryon asymmetry is obtainable only for ultralight PBH of mass $\lesssim 15$ g and RHN mass $M_1 \gtrsim 10^{11}$ GeV. Coincidentally, the same bound on the RHN mass scale is also obtained for the inflaton case discussed before. PBH mass in such a ballpark necessarily requires a prolonged period of PBH domination, typically requiring a large initial fraction $\beta \gtrsim 10^{-3}$. Considering bounds from CMB, BBN and astrophysical constraints, we show that PBH evaporation is also capable of producing required asymmetry in the dark sector leading to correct relic abundance for asymmetric DM as massive as $\sim 10^5$ GeV, depending on the choice of the Yukawa coupling y_χ .

Several complementary prospects of detection for asymmetric DM can be realised depending on the UV completion of the dark sector, which we have not investigated in this minimal setup. In addition to the discovery potential for the particular particle physics framework, the ultra-light PBH leading to early matter domination can itself have observational consequences like emission of gravitational waves via Hawking radiation [141] or other ways [85, 142, 143] which can have interesting detection prospects at both high and low frequency GW experiments [144]. Another interesting future prospects could be to study a complete framework for baryon DMogenesis which incorporate the details of inflationary potential or the origin of ultralight PBHs. We leave such interesting possibilities to future works.

ACKNOWLEDGEMENTS

BB received funding from the Patrimonio Autónomo - Fondo Nacional de Financiamiento para la Ciencia, la Tecnología y la Innovación Francisco José de Caldas (MinCiencias - Colombia) grant 80740-465-2020. This project has received funding /support from the European Union's Horizon 2020 research and innovation programme under the Marie Skłodowska-Curie grant agreement No 860881-HIDDeN.

Appendix A: Light neutrino mass & Casas-Ibarra Parametrisation

The extension of the SM particle spectrum with singlet RHN allows us to write its Yukawa interaction with the SM lepton doublet and Higgs (second term in Eq. (3)). As the neutral component of the SM Higgs doublet acquires a VEV leading to the spontaneous breaking of the SM gauge symmetry, neutrinos in the SM obtain a Dirac mass that can be written as

$$m_D = \frac{y_N}{\sqrt{2}}v. \quad (\text{A1})$$

The Dirac mass m_D together with the RHN bare mass M_N , can explain the nonzero light neutrino masses with the help of Type-I seesaw [37, 39, 145]. Here, the light-neutrino masses can be expressed as,

$$m_\nu \simeq m_D^T M^{-1} m_D. \quad (\text{A2})$$

The mass eigenvalues and mixing are then obtained by diagonalising the light-neutrino mass matrix as

$$m_\nu = \mathcal{U}^* m_\nu^d \mathcal{U}^\dagger, \quad (\text{A3})$$

with $m_\nu^d = \text{dia}(m_1, m_2, m_3)$ consisting of the mass eigenvalues and \mathcal{U} being the Pontecorvo-Maki-Nakagawa-Sakata matrix [6]¹⁴. The interesting aspect of leptogenesis lies in the fact that the same Yukawa couplings involved in neutrino mass generation also play a non-trivial role in determining the lepton asymmetry of the universe as they dictate the decay width of RHNs into the SM leptons. In order to obtain a complex structure of the Yukawa coupling which is essential from the perspective of leptogenesis, we use the well-known Casas-Ibarra (CI) parametrisation [146]. Using this one can write the Yukawa coupling y_N as,

$$y_N = \frac{\sqrt{2}}{v} \sqrt{M} \mathbb{R} \sqrt{m_\nu^d} \mathcal{U}^\dagger, \quad (\text{A4})$$

¹⁴The charged lepton mass matrix is considered to be diagonal.

where \mathbb{R} is a complex orthogonal matrix $\mathbb{R}^T \mathbb{R} = I$, which we choose as

$$\mathbb{R} = \begin{pmatrix} 0 & \cos z & \sin z \\ 0 & -\sin z & \cos z \end{pmatrix}, \quad (\text{A5})$$

where $z = a + ib$ is a complex angle. The above structure of \mathbb{R} can be justified by considering two RHNs or considering the third RHN N_3 to be very heavy and effectively decoupled from the bath. In such a scenario our neutrino Yukawa matrix becomes of dimension 2×3 . Such a scenario also predicts the lightest active neutrino to be exactly massless. The diagonal light neutrino mass matrix m_ν^d is calculable using the best fit values of solar and atmospheric mass obtained from the latest neutrino oscillation data [6]. Now, the elements of Yukawa coupling matrix y_N for a specific value of z , can be obtained for different choices of the heavy neutrino masses. For example, with $M_1 = 10^{12}$ GeV and $\{a, b\} = \{10^{-3}, 10^{-2}\}$ we obtain the following structure

$$y_N = \begin{pmatrix} 0.00913 - 0.00003i & 0.01102 - 0.00052i & -0.00884 - 0.00059i \\ -0.00607 - 0.01209i & 0.05962 - 0.00024i & 0.06772 + 0.00019i \end{pmatrix}, \quad (\text{A6})$$

which satisfies the light neutrino mass, as well as produces desired CP asymmetry in the visible sector, as we discuss below. The complex angle z can be chosen in a way that the CP asymmetry is enhanced, while keeping the Yukawa couplings within perturbative limits.

-
- [1] F. Zwicky, *Helv. Phys. Acta* **6**, 110 (1933), [Gen. Rel. Grav.41,207(2009)].
 - [2] F. Zwicky, *Astrophys. J.* **86**, 217 (1937).
 - [3] V. C. Rubin and W. K. Ford, Jr., *Astrophys. J.* **159**, 379 (1970).
 - [4] D. Clowe, M. Bradac, A. H. Gonzalez, M. Markevitch, S. W. Randall, C. Jones, and D. Zaritsky, *Astrophys. J. Lett.* **648**, L109 (2006), arXiv:astro-ph/0608407.
 - [5] N. Aghanim et al. (Planck), (2018), arXiv:1807.06209 [astro-ph.CO].
 - [6] P. A. Zyla et al. (Particle Data Group), *PTEP* **2020**, 083C01 (2020).
 - [7] A. D. Sakharov, *Pisma Zh. Eksp. Teor. Fiz.* **5**, 32 (1967), [Usp. Fiz. Nauk161,no.5,61(1991)].
 - [8] E. W. Kolb and M. S. Turner, *Front. Phys.* **69**, 1 (1990).

- [9] G. Jungman, M. Kamionkowski, and K. Griest, *Phys. Rept.* **267**, 195 (1996), [arXiv:hep-ph/9506380 \[hep-ph\]](#).
- [10] G. Bertone, D. Hooper, and J. Silk, *Phys. Rept.* **405**, 279 (2005), [arXiv:hep-ph/0404175 \[hep-ph\]](#).
- [11] J. L. Feng, *Ann. Rev. Astron. Astrophys.* **48**, 495 (2010), [arXiv:1003.0904 \[astro-ph.CO\]](#).
- [12] G. Arcadi, M. Dutra, P. Ghosh, M. Lindner, Y. Mambrini, M. Pierre, S. Profumo, and F. S. Queiroz, *Eur. Phys. J. C* **78**, 203 (2018), [arXiv:1703.07364 \[hep-ph\]](#).
- [13] L. Roszkowski, E. M. Sessolo, and S. Trojanowski, *Rept. Prog. Phys.* **81**, 066201 (2018), [arXiv:1707.06277 \[hep-ph\]](#).
- [14] S. Weinberg, *Phys. Rev. Lett.* **42**, 850 (1979).
- [15] E. W. Kolb and S. Wolfram, *Nucl. Phys.* **B172**, 224 (1980), [Erratum: *Nucl. Phys.*B195,542(1982)].
- [16] M. Fukugita and T. Yanagida, *Phys. Lett.* **B174**, 45 (1986).
- [17] V. A. Kuzmin, V. A. Rubakov, and M. E. Shaposhnikov, *Phys. Lett.* **155B**, 36 (1985).
- [18] S. M. Boucenna and S. Morisi, *Front. in Phys.* **1**, 33 (2014), [arXiv:1310.1904 \[hep-ph\]](#).
- [19] S. Nussinov, *Phys. Lett. B* **165**, 55 (1985).
- [20] H. Davoudiasl and R. N. Mohapatra, *New J. Phys.* **14**, 095011 (2012), [arXiv:1203.1247 \[hep-ph\]](#).
- [21] K. Petraki and R. R. Volkas, *Int. J. Mod. Phys. A* **28**, 1330028 (2013), [arXiv:1305.4939 \[hep-ph\]](#).
- [22] K. M. Zurek, *Phys. Rept.* **537**, 91 (2014), [arXiv:1308.0338 \[hep-ph\]](#).
- [23] M. Yoshimura, *Phys. Rev. Lett.* **41**, 281 (1978), [Erratum: *Phys.Rev.Lett.* 42, 746 (1979)].
- [24] S. M. Barr, *Phys. Rev. D* **19**, 3803 (1979).
- [25] I. Baldes, N. F. Bell, K. Petraki, and R. R. Volkas, *Phys. Rev. Lett.* **113**, 181601 (2014), [arXiv:1407.4566 \[hep-ph\]](#).
- [26] Y. Cui, L. Randall, and B. Shuve, *JHEP* **04**, 075 (2012), [arXiv:1112.2704 \[hep-ph\]](#).
- [27] N. Bernal, F.-X. Josse-Michaux, and L. Ubaldi, *JCAP* **01**, 034 (2013), [arXiv:1210.0094 \[hep-ph\]](#).
- [28] N. Bernal, S. Colucci, F.-X. Josse-Michaux, J. Racker, and L. Ubaldi, *JCAP* **10**, 035 (2013), [arXiv:1307.6878 \[hep-ph\]](#).
- [29] J. Kumar and P. Stengel, *Phys. Rev. D* **89**, 055016 (2014), [arXiv:1309.1145 \[hep-ph\]](#).

- [30] J. Racker and N. Rius, *JHEP* **11**, 163 (2014), [arXiv:1406.6105 \[hep-ph\]](#).
- [31] A. Dasgupta, C. Hati, S. Patra, and U. Sarkar, (2016), [arXiv:1605.01292 \[hep-ph\]](#).
- [32] D. Borah, A. Dasgupta, and S. K. Kang, *Eur. Phys. J. C* **80**, 498 (2020), [arXiv:1806.04689 \[hep-ph\]](#).
- [33] D. Borah, A. Dasgupta, and S. K. Kang, *Phys. Rev. D* **100**, 103502 (2019), [arXiv:1903.10516 \[hep-ph\]](#).
- [34] A. Dasgupta, P. S. Bhupal Dev, S. K. Kang, and Y. Zhang, *Phys. Rev. D* **102**, 055009 (2020), [arXiv:1911.03013 \[hep-ph\]](#).
- [35] A. Falkowski, J. T. Ruderman, and T. Volansky, *JHEP* **05**, 106 (2011), [arXiv:1101.4936 \[hep-ph\]](#).
- [36] A. Dutta Banik, R. Roshan, and A. Sil, (2020), [arXiv:2011.04371 \[hep-ph\]](#).
- [37] R. N. Mohapatra and G. Senjanovic, *Phys. Rev. Lett.* **44**, 912 (1980).
- [38] T. Yanagida, Proceedings: Workshop on the Unified Theories and the Baryon Number in the Universe: Tsukuba Conf. Proc. **C7902131**, 95 (1979).
- [39] M. Gell-Mann, P. Ramond, and R. Slansky, Supergravity Workshop Stony Brook, New York, September 27-29, 1979 Conf. Proc. **C790927**, 315 (1979), [arXiv:1306.4669 \[hep-th\]](#).
- [40] S. L. Glashow, Cargese Summer Institute: Quarks and Leptons Cargese, France, July 9-29, 1979, *NATO Sci. Ser. B* **61**, 687 (1980).
- [41] S. Davidson and A. Ibarra, *Phys. Lett. B* **535**, 25 (2002), [arXiv:hep-ph/0202239 \[hep-ph\]](#).
- [42] G. Lazarides and Q. Shafi, *Phys. Lett. B* **258**, 305 (1991).
- [43] H. Murayama, H. Suzuki, T. Yanagida, and J. Yokoyama, *Phys. Rev. Lett.* **70**, 1912 (1993).
- [44] E. W. Kolb, A. D. Linde, and A. Riotto, *Phys. Rev. Lett.* **77**, 4290 (1996), [arXiv:hep-ph/9606260](#).
- [45] G. Giudice, M. Peloso, A. Riotto, and I. Tkachev, *JHEP* **08**, 014 (1999), [arXiv:hep-ph/9905242](#).
- [46] T. Asaka, K. Hamaguchi, M. Kawasaki, and T. Yanagida, *Phys. Lett. B* **464**, 12 (1999), [arXiv:hep-ph/9906366](#).
- [47] T. Asaka, K. Hamaguchi, M. Kawasaki, and T. Yanagida, *Phys. Rev. D* **61**, 083512 (2000), [arXiv:hep-ph/9907559](#).
- [48] K. Hamaguchi, H. Murayama, and T. Yanagida, *Phys. Rev. D* **65**, 043512 (2002), [arXiv:hep-ph/0109030](#).

- [49] R. Jeannerot, S. Khalil, and G. Lazarides, *Phys. Lett. B* **506**, 344 (2001), [arXiv:hep-ph/0103229](#).
- [50] M. Fujii, K. Hamaguchi, and T. Yanagida, *Phys. Rev. D* **65**, 115012 (2002), [arXiv:hep-ph/0202210](#).
- [51] G. Giudice, A. Notari, M. Raidal, A. Riotto, and A. Strumia, *Nucl. Phys. B* **685**, 89 (2004), [arXiv:hep-ph/0310123](#).
- [52] S. Pascoli, S. Petcov, and C. Yaguna, *Phys. Lett. B* **564**, 241 (2003), [arXiv:hep-ph/0301095](#).
- [53] T. Asaka, H. Nielsen, and Y. Takanishi, *Nucl. Phys. B* **647**, 252 (2002), [arXiv:hep-ph/0207023](#).
- [54] G. Panotopoulos, *Phys. Lett. B* **643**, 279 (2006), [arXiv:hep-ph/0606127](#).
- [55] F. Hahn-Woernle and M. Plumacher, *Nucl. Phys. B* **806**, 68 (2009), [arXiv:0801.3972 \[hep-ph\]](#).
- [56] W. Buchmüller, V. Domcke, K. Kamada, and K. Schmitz, (2013), [arXiv:1309.7788 \[hep-ph\]](#).
- [57] D. Croon, N. Fernandez, D. McKeen, and G. White, *JHEP* **06**, 098 (2019), [arXiv:1903.08658 \[hep-ph\]](#).
- [58] D. Borah, S. Jyoti Das, and A. K. Saha, (2020), [arXiv:2005.11328 \[hep-ph\]](#).
- [59] R. Samanta, A. Biswas, and S. Bhattacharya, (2020), [arXiv:2006.02960 \[hep-ph\]](#).
- [60] B. Barman, D. Borah, and R. Roshan, *Phys. Rev. D* **104**, 035022 (2021), [arXiv:2103.01675 \[hep-ph\]](#).
- [61] R. Allahverdi et al., (2020), [10.21105/astro.2006.16182](#), [arXiv:2006.16182 \[astro-ph.CO\]](#).
- [62] W. Abdallah, D. Delepine, and S. Khalil, *Phys. Lett. B* **725**, 361 (2013), [arXiv:1205.1503 \[hep-ph\]](#).
- [63] B. Dutta, C. S. Fong, E. Jimenez, and E. Nardi, *JCAP* **10**, 025 (2018), [arXiv:1804.07676 \[hep-ph\]](#).
- [64] S.-L. Chen, A. Dutta Banik, and Z.-K. Liu, *JCAP* **03**, 009 (2020), [arXiv:1912.07185 \[hep-ph\]](#).
- [65] D. Mahanta and D. Borah, *JCAP* **04**, 032 (2020), [arXiv:1912.09726 \[hep-ph\]](#).
- [66] P. Konar, A. Mukherjee, A. K. Saha, and S. Show, (2020), [arXiv:2007.15608 \[hep-ph\]](#).
- [67] Z.-F. Chang, Z.-X. Chen, J.-S. Xu, and Z.-L. Han, *JCAP* **06**, 006 (2021), [arXiv:2104.02364 \[hep-ph\]](#).
- [68] S. Jyoti Das, D. Mahanta, and D. Borah, (2021), [arXiv:2104.14496 \[hep-ph\]](#).
- [69] A. Kusenko, *Phys. Rept.* **481**, 1 (2009), [arXiv:0906.2968 \[hep-ph\]](#).

- [70] W. Buchmuller, P. Di Bari, and M. Plumacher, *Annals Phys.* **315**, 305 (2005), [arXiv:hep-ph/0401240](#).
- [71] W. Buchmuller, R. D. Peccei, and T. Yanagida, *Ann. Rev. Nucl. Part. Sci.* **55**, 311 (2005), [arXiv:hep-ph/0502169](#).
- [72] M. Kawasaki, K. Kohri, and T. Moroi, *Phys. Rev. D* **71**, 083502 (2005), [arXiv:astro-ph/0408426](#).
- [73] F. Hahn-Woernle and M. Plumacher, *Nucl. Phys. B* **806**, 68 (2009), [arXiv:0801.3972 \[hep-ph\]](#).
- [74] M. A. G. Garcia, K. Kaneta, Y. Mambrini, and K. A. Olive, *Phys. Rev. D* **101**, 123507 (2020), [arXiv:2004.08404 \[hep-ph\]](#).
- [75] P. Di Bari, *Nucl. Phys. B* **727**, 318 (2005), [arXiv:hep-ph/0502082](#).
- [76] G. F. Giudice, E. W. Kolb, and A. Riotto, *Phys. Rev. D* **64**, 023508 (2001), [arXiv:hep-ph/0005123](#).
- [77] Y. Akrami *et al.* (Planck), *Astron. Astrophys.* **641**, A10 (2020), [arXiv:1807.06211 \[astro-ph.CO\]](#).
- [78] B. Carr, K. Kohri, Y. Sendouda, and J. Yokoyama, (2020), [arXiv:2002.12778 \[astro-ph.CO\]](#).
- [79] T. Fujita, M. Kawasaki, K. Harigaya, and R. Matsuda, *Phys. Rev. D* **89**, 103501 (2014), [arXiv:1401.1909 \[astro-ph.CO\]](#).
- [80] I. Masina, *Eur. Phys. J. Plus* **135**, 552 (2020), [arXiv:2004.04740 \[hep-ph\]](#).
- [81] S. W. Hawking, *Nature* **248**, 30 (1974).
- [82] S. W. Hawking, *Commun. Math. Phys.* **43**, 199 (1975), [Erratum: *Commun.Math.Phys.* 46, 206 (1976)].
- [83] J. H. MacGibbon, *Phys. Rev. D* **44**, 376 (1991).
- [84] N. Bernal and O. Zapata, *JCAP* **03**, 015 (2021), [arXiv:2011.12306 \[astro-ph.CO\]](#).
- [85] T. Papanikolaou, V. Vennin, and D. Langlois, *JCAP* **03**, 053 (2021), [arXiv:2010.11573 \[astro-ph.CO\]](#).
- [86] B. Carr and F. Kuhnel, *Ann. Rev. Nucl. Part. Sci.* **70**, 355 (2020), [arXiv:2006.02838 \[astro-ph.CO\]](#).
- [87] G. F. Chapline, *Nature* **253**, 251 (1975).
- [88] B. J. Carr, *Astrophys. J.* **206**, 8 (1976).
- [89] N. Smyth, L. Santos-Olmsted, and S. Profumo, (2021), [arXiv:2110.14660 \[hep-ph\]](#).
- [90] D. Baumann, P. J. Steinhardt, and N. Turok, (2007), [arXiv:hep-th/0703250](#).

- [91] A. Hook, *Phys. Rev. D* **90**, 083535 (2014), arXiv:1404.0113 [hep-ph].
- [92] Y. Hamada and S. Iso, *PTEP* **2017**, 033B02 (2017), arXiv:1610.02586 [hep-ph].
- [93] L. Morrison, S. Profumo, and Y. Yu, *JCAP* **05**, 005 (2019), arXiv:1812.10606 [astro-ph.CO].
- [94] D. Hooper and G. Krnjaic, *Phys. Rev. D* **103**, 043504 (2021), arXiv:2010.01134 [hep-ph].
- [95] Y. F. Perez-Gonzalez and J. Turner, (2020), arXiv:2010.03565 [hep-ph].
- [96] S. Datta, A. Ghosal, and R. Samanta, *JCAP* **08**, 021 (2021), arXiv:2012.14981 [hep-ph].
- [97] V. De Luca, G. Franciolini, A. Kehagias, and A. Riotto, *Phys. Lett. B* **819**, 136454 (2021), arXiv:2102.07408 [astro-ph.CO].
- [98] P. Gondolo, P. Sandick, and B. Shams Es Haghi, *Phys. Rev. D* **102**, 095018 (2020), arXiv:2009.02424 [hep-ph].
- [99] N. Bernal, Y. F. Perez-Gonzalez, Y. Xu, and O. Zapata, (2021), arXiv:2110.04312 [hep-ph].
- [100] N. Bernal, F. Hajkarim, and Y. Xu, *Phys. Rev. D* **104**, 075007 (2021), arXiv:2107.13575 [hep-ph].
- [101] D. Hooper, G. Krnjaic, and S. D. McDermott, *JHEP* **08**, 001 (2019), arXiv:1905.01301 [hep-ph].
- [102] C. Lunardini and Y. F. Perez-Gonzalez, *JCAP* **08**, 014 (2020), arXiv:1910.07864 [hep-ph].
- [103] F. Schiavone, D. Montanino, A. Mirizzi, and F. Capozzi, *JCAP* **08**, 063 (2021), arXiv:2107.03420 [hep-ph].
- [104] A. M. Green, *Phys. Rev. D* **60**, 063516 (1999), arXiv:astro-ph/9903484.
- [105] M. Y. Khlopov, A. Barrau, and J. Grain, *Class. Quant. Grav.* **23**, 1875 (2006), arXiv:astro-ph/0406621.
- [106] D.-C. Dai, K. Freese, and D. Stojkovic, *JCAP* **06**, 023 (2009), arXiv:0904.3331 [hep-ph].
- [107] R. Allahverdi, J. Dent, and J. Osinski, *Phys. Rev. D* **97**, 055013 (2018), arXiv:1711.10511 [astro-ph.CO].
- [108] O. Lennon, J. March-Russell, R. Petrossian-Byrne, and H. Tillim, *JCAP* **04**, 009 (2018), arXiv:1712.07664 [hep-ph].
- [109] A. Chaudhuri and A. Dolgov, (2020), arXiv:2001.11219 [astro-ph.CO].
- [110] I. Baldes, Q. Decant, D. C. Hooper, and L. Lopez-Honorez, *JCAP* **08**, 045 (2020), arXiv:2004.14773 [astro-ph.CO].
- [111] N. Bernal and O. Zapata, *Phys. Lett. B* **815**, 136129 (2021), arXiv:2011.02510 [hep-ph].
- [112] B. C. Lacki and J. F. Beacom, *Astrophys. J. Lett.* **720**, L67 (2010), arXiv:1003.3466 [astro-

- ph.CO].
- [113] S. M. Boucenna, F. Kuhnel, T. Ohlsson, and L. Visinelli, *JCAP* **07**, 003 (2018), [arXiv:1712.06383 \[hep-ph\]](#).
- [114] J. Adamek, C. T. Byrnes, M. Gosenca, and S. Hotchkiss, *Phys. Rev. D* **100**, 023506 (2019), [arXiv:1901.08528 \[astro-ph.CO\]](#).
- [115] B. Carr, F. Kuhnel, and L. Visinelli, *Mon. Not. Roy. Astron. Soc.* **506**, 3648 (2021), [arXiv:2011.01930 \[astro-ph.CO\]](#).
- [116] I. Masina, (2021), [arXiv:2103.13825 \[gr-qc\]](#).
- [117] P. Sandick, B. S. Es Haghi, and K. Sinha, *Phys. Rev. D* **104**, 083523 (2021), [arXiv:2108.08329 \[astro-ph.CO\]](#).
- [118] A. Cheek, L. Heurtier, Y. F. Perez-Gonzalez, and J. Turner, (2021), [arXiv:2107.00016 \[hep-ph\]](#).
- [119] A. Cheek, L. Heurtier, Y. F. Perez-Gonzalez, and J. Turner, (2021), [arXiv:2107.00013 \[hep-ph\]](#).
- [120] V. Iršič *et al.*, *Phys. Rev. D* **96**, 023522 (2017), [arXiv:1702.01764 \[astro-ph.CO\]](#).
- [121] G. Ballesteros, M. A. G. Garcia, and M. Pierre, *JCAP* **03**, 101 (2021), [arXiv:2011.13458 \[hep-ph\]](#).
- [122] F. D’Eramo and A. Lenoci, (2020), [arXiv:2012.01446 \[hep-ph\]](#).
- [123] R. Diamanti, S. Ando, S. Gariazzo, O. Mena, and C. Weniger, *JCAP* **06**, 008 (2017), [arXiv:1701.03128 \[astro-ph.CO\]](#).
- [124] K. Inomata, K. Kohri, T. Nakama, and T. Terada, *Phys. Rev. D* **100**, 043532 (2019), [arXiv:1904.12879 \[astro-ph.CO\]](#).
- [125] G. Domènech, V. Takhistov, and M. Sasaki, *Phys. Lett. B* **823**, 136722 (2021), [arXiv:2105.06816 \[astro-ph.CO\]](#).
- [126] A. Caputo, A. J. Millar, C. A. J. O’Hare, and E. Vitagliano, (2021), [arXiv:2105.04565 \[hep-ph\]](#).
- [127] K. Griest and M. Kamionkowski, *Phys. Rev. Lett.* **64**, 615 (1990).
- [128] E. C. G. Stueckelberg, *Helv. Phys. Acta* **11**, 225 (1938).
- [129] M. Kaplinghat, S. Tulin, and H.-B. Yu, *Phys. Rev. D* **89**, 035009 (2014), [arXiv:1310.7945 \[hep-ph\]](#).
- [130] S. Tulin and H.-B. Yu, *Phys. Rept.* **730**, 1 (2018), [arXiv:1705.02358 \[hep-ph\]](#).

- [131] M. Dutta, S. Mahapatra, D. Borah, and N. Sahu, *Phys. Rev. D* **103**, 095018 (2021), [arXiv:2101.06472 \[hep-ph\]](#).
- [132] D. Borah, M. Dutta, S. Mahapatra, and N. Sahu, (2021), [arXiv:2107.13176 \[hep-ph\]](#).
- [133] D. Borah, M. Dutta, S. Mahapatra, and N. Sahu, (2021), [arXiv:2110.00021 \[hep-ph\]](#).
- [134] R. Jinno and M. Takimoto, *Phys. Rev. D* **95**, 015020 (2017), [arXiv:1604.05035 \[hep-ph\]](#).
- [135] C.-W. Chiang and E. Senaha, *Phys. Lett. B* **774**, 489 (2017), [arXiv:1707.06765 \[hep-ph\]](#).
- [136] K. Hashino, M. Kakizaki, S. Kanemura, P. Ko, and T. Matsui, *JHEP* **06**, 088 (2018), [arXiv:1802.02947 \[hep-ph\]](#).
- [137] T. Hasegawa, N. Okada, and O. Seto, *Phys. Rev. D* **99**, 095039 (2019), [arXiv:1904.03020 \[hep-ph\]](#).
- [138] A. Mohamadnejad, *Eur. Phys. J. C* **80**, 197 (2020), [arXiv:1907.08899 \[hep-ph\]](#).
- [139] Y. G. Kim, K. Y. Lee, and S.-H. Nam, *Phys. Rev. D* **100**, 075038 (2019), [arXiv:1906.03390 \[hep-ph\]](#).
- [140] D. Borah, A. Dasgupta, and S. K. Kang, *Phys. Rev. D* **104**, 063501 (2021), [arXiv:2105.01007 \[hep-ph\]](#).
- [141] R. Anantua, R. Easther, and J. T. Giblin, *Phys. Rev. Lett.* **103**, 111303 (2009), [arXiv:0812.0825 \[astro-ph\]](#).
- [142] R. Saito and J. Yokoyama, *Phys. Rev. Lett.* **102**, 161101 (2009), [Erratum: *Phys.Rev.Lett.* 107, 069901 (2011)], [arXiv:0812.4339 \[astro-ph\]](#).
- [143] D. Hooper, G. Krnjaic, J. March-Russell, S. D. McDermott, and R. Petrossian-Byrne, (2020), [arXiv:2004.00618 \[astro-ph.CO\]](#).
- [144] J. Kozaczuk, T. Lin, and E. Villarama, (2021), [arXiv:2108.12475 \[astro-ph.CO\]](#).
- [145] P. Minkowski, *Physics Letters B* **67**, 421 (1977).
- [146] J. A. Casas and A. Ibarra, *Nucl. Phys. B* **618**, 171 (2001), [arXiv:hep-ph/0103065](#).